

Lodz University of Technology

SCIENTIFIC BULLETIN

PHYSICS

Vol. 34

LODZ 2013

LODZ UNIVERSITY OF TECHNOLOGY

SCIENTIFIC BULLETIN

No. 1183

PHYSICS

Vol. 34

LODZ 2013

ZESZYTY NAUKOWE POLITECHNIKI ŁÓDZKIEJ
SCIENTIFIC BULLETIN OF THE LODZ UNIVERSITY OF TECHNOLOGY
BULLETIN SCIENTIFIQUE
DE L'UNIVERSITÉ POLYTECHNIQUE DE LODZ
НАУЧНЫЕ ЗАПИСКИ
ЛОДЗИНСКОГО ПОЛИТЕХНИЧЕСКОГО УНИВЕРСИТЕТА
WISSENSCHAFTLICHE HEFTE
DER TECHNISCHEN UNIVERSITÄT IN LODZ

Editor of series: **Assoc. Professor Grzegorz Derfel, Ph.D., D.Sc.**
Subject Editor of series: **Assoc. Professor Mirosława Rak, Ph.D., D.Sc.**
Secretary of series: **Marek Wojciechowski, Ph.D.**

Printed version of the journal is the main version

© Copyright by Politechnika Łódzka 2013

Adres Redakcji – Адрес Редакции – Editor's Office
Adresse de Redaction – Schriftleitungsadresse:

WYDAWNICTWO POLITECHNIKI ŁÓDZKIEJ
90-924 Łódź, ul. Wólczańska 223
tel./fax 42-684-07-93
e-mail: zamówienia@info.p.lodz.pl
www.wydawnictwa.p.lodz.pl

ISSN 1505-1013

Nakład 100 egz. Ark. druk. 4,0. Papier offset. 80 g 70 x 100
Druk ukończono w lutym 2014 r.
Wykonano w Drukarni Offsetowej Quick-Druk, 90-562 Łódź, ul. Łąkowa

CONTENTS

Marek Izdebski, Rafał Ledzion, Włodzimierz Kucharczyk – Analysis of measurement of quadratic electro-optic effect in castor oil	5
Sylwester Kania – Hole drift mobility for different structures of anthrone and anthracinone layers	19
Sylwester Kania, Janusz Kuliński – Adsorption of ethanol to thin layer of acenes as a process of interconnected networks	27
Sylwester Kania, Janusz Kuliński, Bernard Marciniak, Ewa Różycka-Sokolowska – Some electrical properties of thin layers of 9,10-dimethylantracene and 1-acenaphthenol	35
Rafał Ledzion, Marek Izdebski, Piotr Górski, Włodzimierz Kucharczyk – Estimations of the magnitude of the fourth-order electrooptic effect in KDP-type crystals	43
Magdalena Włodarska, Bartosz Skurpel – Curing conditions and dielectric observation of an epoxy system based on epidian 6	49
Marek Wojciechowski, Marzena Tykarska, Grzegorz W. Bąk – Dielectric properties of ferroelectric subphase of liquid crystal MHPOPB	57

MAREK IZDEBSKI, RAFAŁ LEDZION
WŁODZIMIERZ KUCHARCZYK

Institute of Physics, Lodz University of Technology
ul. Wólczajska 219, 90-924 Łódź, Poland, e-mail: izdebski@p.lodz.pl

ANALYSIS OF MEASUREMENT OF QUADRATIC ELECTRO-OPTIC EFFECT IN CASTOR OIL

This work presents an extended theoretical analysis of the response of experimental setup to an applied electric field during measurements of electro-optic coefficients in optically active liquids using an optical polarimetric technique. The analysis includes liquids belonging to $\infty\infty$, $\infty 2$ and ∞ Curie symmetry groups and the following phenomena were taken into account: natural optical activity, natural linear birefringence, dichroism, and the effects induced by an applied electric field – linear and quadratic electro-optic effects and linear and quadratic electrogyration. The presented example concerns numerical error analysis for measurement of the quadratic electro-optic effect in castor oil, which exhibits the symmetry $\infty 2$ between a pair of plane-parallel electrodes.

Keywords: castor oil, electro-optic effects, optical activity, dichroism.

1. INTRODUCTION

The recent results have shown that the measurements of the Kerr constant and its temperature dependence are useful in the study of castor oil aging [1]. A simplified analysis of optical response of the measurement system to the applied external electric field presented previously was derived for an isotropic liquid belonging to the $\infty\infty m$ Curie group symmetry, which excludes the dichroism, natural linear birefringence, natural optical activity, and the optical activity induced by the applied electric field (also called electrogyration effect). The castor oil, however, is known for its natural optical activity 4-6°/dm [2], which means, that the internal symmetry of the oil must be described by one of the three Curie groups allowing for this phenomenon: $\infty\infty$, $\infty 2$ or ∞ . Recent studies

have also shown that the correct description of the optical properties of the castor oil between a pair of metal plane-parallel plates with a several millimetres space between them requires consideration of the circular birefringence, linear birefringence, and dichroism occurring at the same time, which means that the oil symmetry can be described only by the $\infty 2$ or ∞ groups [3]. The previous study concerned the interaction between the oil and material of plates in the absence of any applied electric or magnetic field, which did not give any possibility to distinguish between the $\infty 2$ and ∞ groups. However, in the case of measurements with an externally applied field the two symmetries lead to substantially different optical responses.

The aim of this work is to provide an extended theoretical analysis of the optical response to an applied electric field, which appears in the experimental setup employed in measurements of electro-optic coefficients using the optical polarimetric method. The analysis includes the dichroism, natural linear birefringence, natural optical activity and the effects induced by an applied electric field, namely the linear and quadratic electro-optic effects and the linear and quadratic electrogyration. The consequences of transitions between the $\infty\infty$, $\infty 2$ and ∞ symmetries in the sample of liquid are also discussed. Moreover, the measurement conditions were identified in which the manifestation of undesirable effects should not significantly disturb the measurements of electro-optic coefficients. Although this work refers to the measurements in the castor oil, the presented extended analysis may be useful to better understanding of measurements with many other optically active liquids.

2. THEORETICAL ANALYSIS

2.1. Impermeability tensor for optically active liquids

Let us consider any dichroic homogeneous nonmagnetic nondepolarizing elliptically birefringent liquid. The electro-optic effects are defined in terms of changes in the real part of the optical frequency impermeability tensor $[B_{ij}]$ caused by an applied electric field \mathbf{E}

$$\text{Re}[B_{ij}] = \text{Re}[B_{ij}^{(0)}] + r_{ijk} E_k + q_{ijkl} E_k E_l + \dots, \quad (1)$$

where $\text{Re}[B_{ij}^{(0)}]$ are the field-free components of the tensor related to the natural linear birefringence, r_{ijk} are the components of the linear electro-optic tensor, and q_{ijkl} are the components of the quadratic electro-optic tensors (Table 1). The real part $\text{Re}[B_{ij}]$ is exactly symmetrical only for non-absorbing media, but the asymmetry associated with the absorption is typically negligibly small and will

be omitted in this work. As the absorption should be taken into account in this study, we use the transmission coefficients, which are not explicitly related to the $[B_{ij}]$ tensor.

The imaginary antisymmetric part of the $[B_{ij}]$ tensor represents the optical activity, however, traditionally the optical activity is described with the relative electric permittivity tensor $[K_{ij}]$. The imaginary antisymmetric part of the $[K_{ij}]$ tensor can be written as [4]

$$\text{Im}[K_{ij}] = \begin{bmatrix} 0 & -G_3 & G_2 \\ G_3 & 0 & -G_1 \\ -G_2 & G_1 & 0 \end{bmatrix}, \quad (2)$$

where G_1 , G_2 and G_3 are the elements of the gyration vector \mathbf{G} for a given wave propagation vector \mathbf{s}

$$\mathbf{G} = [g]\mathbf{s}. \quad (3)$$

In Eq. (3) $[g]$ is a second rank gyration axial tensor described by a real 3×3 matrix. The total optical activity of a liquid exhibiting the natural optical activity and the activity induced by a DC or low-frequency electric field can be expressed by the following power series

$$g_{ij} = g_{ij}^{(0)} + \gamma_{ijk} E_k + \beta_{ijkl} E_k E_l + \dots, \quad (4)$$

where $g_{ij}^{(0)}$ are the components of field-free gyration tensor describing a natural optical activity, γ_{ijk} are the components of the linear electrogyration tensors, and β_{ijkl} are the components of the quadratic electrogyration tensor (Table 2). The imaginary antisymmetric part of $[B]$ may be found using the formula which follows from the definition of the impermeability tensor $[B] = [K]^{-1}$ [5]

$$\text{Im}[B] = -(\text{Re}[B])(\text{Im}[K])(\text{Re}[B]). \quad (5)$$

The formulas (1)-(5) allow us to find the total complex Hermitian tensor $[B]$ for a given directions of the light and applied electric field.

A pair of plane-parallel electrodes immersed in castor oil induce a dichroism and linear birefringence, with the optical axis directed perpendicularly to the electrodes [3]. Thus, the formulas (1)-(5) and Tables 1 and 2 are written for such XYZ coordinates, where the Z axis is associated with the applied electric field $\mathbf{E} = [0, 0, E]$, and the X and Y axes can be chosen freely. In calculations of the light transmission through the system of plane-parallel plates we use, however, another coordinate system $X'Y'Z'$, in which the direction of the light beam \mathbf{s} defines the $+Z'$ axis and the direction of the field $\mathbf{E} \parallel X'$.

Table 1

The real part of the impermeability tensor $[B_{ij}]$ for optically active liquids in the presence of an electric field \mathbf{E} [6]. For all the groups included in the table $q_{66} = \frac{1}{2}(q_{11} - q_{12})$

Natural linear birefringence $B_{ij}^{(0)}$			Linear electro-optic r_{ijk}			Quadratic electro-optic q_{ijkl}					
$\text{Re}[B_{ij}] = B_{ij}^{(0)} + r_{ijk}E_k + q_{ijkl}E_kE_l + \dots$											
$\infty\infty$ Curie group											
$\begin{bmatrix} n_{01}^{-2} & 0 & 0 \\ 0 & n_{01}^{-2} & 0 \\ 0 & 0 & n_{01}^{-2} \end{bmatrix}$			$\begin{bmatrix} 0 & 0 & 0 \\ 0 & 0 & 0 \\ 0 & 0 & 0 \\ 0 & 0 & 0 \\ 0 & 0 & 0 \\ 0 & 0 & 0 \end{bmatrix}$			$\begin{bmatrix} q_{11} & q_{12} & q_{12} & 0 & 0 & 0 \\ q_{12} & q_{11} & q_{12} & 0 & 0 & 0 \\ q_{12} & q_{12} & q_{11} & 0 & 0 & 0 \\ 0 & 0 & 0 & q_{44} & 0 & 0 \\ 0 & 0 & 0 & 0 & q_{44} & 0 \\ 0 & 0 & 0 & 0 & 0 & q_{44} \end{bmatrix}$					
$\infty 2$ Curie group											
$\begin{bmatrix} n_{01}^{-2} & 0 & 0 \\ 0 & n_{01}^{-2} & 0 \\ 0 & 0 & n_{03}^{-2} \end{bmatrix}$			$\begin{bmatrix} 0 & 0 & 0 \\ 0 & 0 & 0 \\ 0 & 0 & 0 \\ r_{41} & 0 & 0 \\ 0 & -r_{41} & 0 \\ 0 & 0 & 0 \end{bmatrix}$			$\begin{bmatrix} q_{11} & q_{12} & q_{13} & 0 & 0 & 0 \\ q_{12} & q_{11} & q_{13} & 0 & 0 & 0 \\ q_{31} & q_{31} & q_{33} & 0 & 0 & 0 \\ 0 & 0 & 0 & q_{44} & 0 & 0 \\ 0 & 0 & 0 & 0 & q_{44} & 0 \\ 0 & 0 & 0 & 0 & 0 & q_{66} \end{bmatrix}$					
∞ Curie group											
$\begin{bmatrix} n_{01}^{-2} & 0 & 0 \\ 0 & n_{01}^{-2} & 0 \\ 0 & 0 & n_{03}^{-2} \end{bmatrix}$			$\begin{bmatrix} 0 & 0 & r_{13} \\ 0 & 0 & r_{13} \\ 0 & 0 & r_{33} \\ r_{41} & r_{51} & 0 \\ r_{51} & -r_{41} & 0 \\ 0 & 0 & 0 \end{bmatrix}$			$\begin{bmatrix} q_{11} & q_{12} & q_{13} & 0 & 0 & q_{16} \\ q_{12} & q_{11} & q_{13} & 0 & 0 & -q_{16} \\ q_{31} & q_{31} & q_{33} & 0 & 0 & 0 \\ 0 & 0 & 0 & q_{44} & q_{45} & 0 \\ 0 & 0 & 0 & -q_{45} & q_{44} & 0 \\ -q_{16} & q_{16} & 0 & 0 & 0 & q_{66} \end{bmatrix}$					

Table 2

The gyration tensor $[g_{ij}]$ for optically active liquids in the presence of an electric field \mathbf{E} [6]. For all the groups included in the table $\beta_{66} = \frac{1}{2}(\beta_{11} - \beta_{12})$

$g_{ij} = g_{ij}^{(0)} + \gamma_{ijk}E_k + \beta_{ijkl}E_kE_l + \dots$		
Natural optical activity $g_{ij}^{(0)}$	Linear electrogyration γ_{ijk}	Quadratic electrogyration β_{ijkl}
$\infty\infty$ Curie group		
$\begin{bmatrix} g_{11}^{(0)} & 0 & 0 \\ 0 & g_{11}^{(0)} & 0 \\ 0 & 0 & g_{11}^{(0)} \end{bmatrix}$	$\begin{bmatrix} 0 & 0 & 0 \\ 0 & 0 & 0 \\ 0 & 0 & 0 \\ 0 & 0 & 0 \\ 0 & 0 & 0 \\ 0 & 0 & 0 \end{bmatrix}$	$\begin{bmatrix} \beta_{11} & \beta_{12} & \beta_{12} & 0 & 0 & 0 \\ \beta_{12} & \beta_{11} & \beta_{12} & 0 & 0 & 0 \\ \beta_{12} & \beta_{12} & \beta_{11} & 0 & 0 & 0 \\ 0 & 0 & 0 & \beta_{44} & 0 & 0 \\ 0 & 0 & 0 & 0 & \beta_{44} & 0 \\ 0 & 0 & 0 & 0 & 0 & \beta_{44} \end{bmatrix}$
$\infty 2$ Curie group		
$\begin{bmatrix} g_{11}^{(0)} & 0 & 0 \\ 0 & g_{11}^{(0)} & 0 \\ 0 & 0 & g_{33}^{(0)} \end{bmatrix}$	$\begin{bmatrix} 0 & 0 & 0 \\ 0 & 0 & 0 \\ 0 & 0 & 0 \\ \gamma_{41} & 0 & 0 \\ 0 & -\gamma_{41} & 0 \\ 0 & 0 & 0 \end{bmatrix}$	$\begin{bmatrix} \beta_{11} & \beta_{12} & \beta_{13} & 0 & 0 & 0 \\ \beta_{12} & \beta_{11} & \beta_{13} & 0 & 0 & 0 \\ \beta_{31} & \beta_{31} & \beta_{33} & 0 & 0 & 0 \\ 0 & 0 & 0 & \beta_{44} & 0 & 0 \\ 0 & 0 & 0 & 0 & \beta_{44} & 0 \\ 0 & 0 & 0 & 0 & 0 & \beta_{66} \end{bmatrix}$
∞ Curie group		
$\begin{bmatrix} g_{11}^{(0)} & 0 & 0 \\ 0 & g_{11}^{(0)} & 0 \\ 0 & 0 & g_{33}^{(0)} \end{bmatrix}$	$\begin{bmatrix} 0 & 0 & \gamma_{13} \\ 0 & 0 & \gamma_{13} \\ 0 & 0 & \gamma_{33} \\ \gamma_{41} & \gamma_{51} & 0 \\ \gamma_{51} & -\gamma_{41} & 0 \\ 0 & 0 & 0 \end{bmatrix}$	$\begin{bmatrix} \beta_{11} & \beta_{12} & \beta_{13} & 0 & 0 & \beta_{16} \\ \beta_{12} & \beta_{11} & \beta_{13} & 0 & 0 & -\beta_{16} \\ \beta_{31} & \beta_{31} & \beta_{33} & 0 & 0 & 0 \\ 0 & 0 & 0 & \beta_{44} & \beta_{45} & 0 \\ 0 & 0 & 0 & -\beta_{45} & \beta_{44} & 0 \\ -\beta_{16} & \beta_{16} & 0 & 0 & 0 & \beta_{66} \end{bmatrix}$

The total $[B']$ tensor derived from Eqs. (1)-(5) and transformed to the $X'Y'Z'$ coordinates has the following form dependent on the Curie group:

1) the $\infty\infty$ symmetry

$$[B'] = \begin{bmatrix} n_{01}^{-2} + q_{11}E^2 & B'_{12} & 0 \\ -B'_{12} & n_{01}^{-2} + q_{12}E^2 & 0 \\ 0 & 0 & n_{01}^{-2} + q_{12}E^2 \end{bmatrix},$$

$$B'_{12} = i n_{01}^{-4} (g_{11}^{(0)} + \beta_{12}E^2) + i n_{01}^{-2} g_{11}^{(0)} (q_{11} + q_{12})E^2, \quad (6)$$

2) the $\infty 2$ symmetry

$$[B'] = \begin{bmatrix} n_{03}^{-2} + q_{33}E^2 & B'_{12} & 0 \\ -B'_{12} & n_{01}^{-2} + q_{13}E^2 & 0 \\ 0 & 0 & n_{03}^{-2} + q_{13}E^2 \end{bmatrix},$$

$$B'_{12} = i n_{01}^{-2} n_{03}^{-2} (g_{11}^{(0)} + \beta_{13}E^2) + i g_{11}^{(0)} (n_{01}^{-2} q_{33} + n_{03}^{-2} q_{13})E^2, \quad (7)$$

3) the ∞ symmetry

$$[B'] = \begin{bmatrix} n_{03}^{-2} + r_{33}E + q_{33}E^2 & B'_{12} & 0 \\ -B'_{12} & n_{01}^{-2} + r_{13}E + q_{13}E^2 & 0 \\ 0 & 0 & n_{03}^{-2} + r_{13}E + q_{13}E^2 \end{bmatrix},$$

$$B'_{12} = i n_{01}^{-2} n_{03}^{-2} (g_{11}^{(0)} + \gamma_{13}E + \beta_{13}E^2) + i (g_{11}^{(0)} + \gamma_{13}E) (n_{01}^{-2} r_{33} + n_{03}^{-2} r_{13})E +$$

$$+ i g_{11}^{(0)} (n_{01}^{-2} q_{33} + n_{03}^{-2} q_{13} + r_{13} r_{33})E^2, \quad (8)$$

where the contribution of the products of $g_{11}^{(0)}$ and electro-optic coefficients is negligible compared to the products of n_{01}^{-2} , n_{03}^{-2} and the electrogyration coefficients.

2.2. Light modulation in measurement system

The intensity of the light emerging from the system of plane-parallel plates has been derived using the Jones calculus. To describe the transition of the light through a single plate we have used one of the most general forms of the Jones M-matrix, valid for any dichroic homogeneous elliptically birefringent medium, which has been derived by Ścierski & Ratajczyk [7]. The matrix was originally written with the use of variables that characterize the polarization of the light

waves propagating in the medium. Next, the matrix written in the form explicitly depending on the $[B]$ complex Hermitian tensor has been presented recently in Ref. [8].

Let us consider a typical experimental setup for the measurements of electro-optic coefficients based on the optical polarimetric method, which consists of the following elements arranged in the following order: a linear polarizer of the azimuth $\alpha_p = \pm 45^\circ$ (relative to $+X'$ axis, which defines the reference zero azimuth), a quarter-wave plate of the azimuth $\alpha_{\lambda/4} = 0^\circ$ or 90° (for the fast wave), a cuvette with an optically active liquid and immersed electrodes, and a linear analyzer of any arbitrary azimuth α_a . The intensity I of the light passing through the system relative to the intensity I_p behind the polarizer derived by the Jones calculus may be written as:

$$\begin{aligned} \frac{I}{I_p} = & \frac{1}{4}(T_f^2 + T_s^2) + \\ & + \frac{1}{4}(T_f^2 - T_s^2) \frac{(B'_{11} - B'_{22}) \cos(2\alpha_a) \pm z 2 \operatorname{Im}[B'_{12}]}{\sqrt{(B'_{11} - B'_{22})^2 + 4B'_{12}B'_{12}^*}} + \\ & \pm z \frac{1}{2} \cos(2\alpha_a) \frac{(B'_{11} - B'_{22}) \operatorname{Im}[B'_{12}]}{(B'_{11} - B'_{22})^2 + 4B'_{12}B'_{12}^*} (T_f^2 + T_s^2 - 2T_f T_s \cos \Gamma) + \\ & \mp z \frac{1}{2} \sin(2\alpha_a) T_f T_s \frac{B'_{11} - B'_{22}}{\sqrt{(B'_{11} - B'_{22})^2 + 4B'_{12}B'_{12}^*}} \sin \Gamma, \end{aligned} \quad (9)$$

where the symbol $*$ indicates the complex conjugate, the upper signs in the “ \mp ” and “ \pm ” symbols correspond to $\alpha_p = +45^\circ$ and the lower signs to $\alpha_p = -45^\circ$, $z = +1$ for $\alpha_{\lambda/4} = 0^\circ$ and $z = -1$ for 90° , T_f and T_s are the amplitude transmission coefficients for the fast and slow waves, respectively, and Γ is the phase difference between the slow and fast waves. It can be seen from Eq. (9) that turning the polarizer between the azimuths $+45^\circ$ and -45° gives an equivalent effect as changing $\alpha_{\lambda/4}$ between 0° and 90° .

When the cuvette contains an optically active medium, the order of the quarter-wave plate and the cuvette is important. If the quarter-wave plate is placed behind the cuvette the following formula applies:

$$\begin{aligned}
\frac{I}{I_p} = & \frac{1}{4}(T_f^2 + T_s^2) + \\
& + \frac{1}{4}(T_f^2 - T_s^2) \frac{(B'_{11} - B'_{22}) \cos(2\alpha_a) - 2z \operatorname{Im}[B'_{12}] \sin(2\alpha_a)}{\sqrt{(B'_{11} - B'_{22})^2 + 4B'_{12}B'_{12}^*}} + \\
& \mp \cos(2\alpha_a) T_f T_s \frac{\operatorname{Im}[B'_{12}]}{\sqrt{(B'_{11} - B'_{22})^2 + 4B'_{12}B'_{12}^*}} \sin \Gamma + \\
& \mp z \frac{1}{2} \sin(2\alpha_a) T_f T_s \frac{B'_{11} - B'_{22}}{\sqrt{(B'_{11} - B'_{22})^2 + 4B'_{12}B'_{12}^*}} \sin \Gamma,
\end{aligned} \tag{10}$$

where the upper and lower signs in “ \mp ” and the symbol z has the same meaning as in Eq. (9). In Eqs. (9) and (10) we omitted for brevity the terms containing $\operatorname{Re}[B'_{12}]$, which vanish for all forms of the $[B]$ tensor given by Eqs. (6)-(8). The phase difference in Eqs. (9) and (10) is given by

$$\Gamma = \frac{2\pi l}{\lambda} (n_s - n_f), \tag{11}$$

where λ is the wavelength of the light, l is the light path-length between electrodes in the cuvette, and n_f and n_s are the refractive indices of the fast and slow waves, respectively. The refractive indices of the liquid described by the complex Hermitian impermeability tensor can be found by employing the formulas [8]

$$n_f = \sqrt{\frac{2}{B'_{11} + B'_{22} + \sqrt{(B'_{11} - B'_{22})^2 + 4B'_{12}B'_{12}^*}}}, \tag{12}$$

$$n_s = \sqrt{\frac{2}{B'_{11} + B'_{22} - \sqrt{(B'_{11} - B'_{22})^2 + 4B'_{12}B'_{12}^*}}}. \tag{13}$$

It is known from experiments that the difference between the field-free refractive indices $n_{01} - n_{03}$ is very small in comparison to n_{01} and n_{03} (for castor oil between stainless steel plates at room temperature: $|n_{01} - n_{03}| \approx 1.6 \cdot 10^{-7}$ and $n_{01} \approx n_{03} \approx 1.48$ [3]), thus the expressions $n_{01} n_{03}$ and $n_{01} + n_{03}$ may be written using the average value $n_0 = (n_{01} + n_{03})/2$. Moreover, the relation $B'_{11} + B'_{22} \gg$

$\sqrt{(B'_{11} - B'_{22})^2 + 4B'_{12}B'_{12}^*}$ enables the following approximations

$$\Gamma \approx \frac{2\sqrt{2}\pi l}{\lambda} \frac{\sqrt{(B'_{11} - B'_{22})^2 + 4B'_{12}B'_{12}^*}}{(B'_{11} + B'_{22})^{3/2}} \approx \frac{\pi l n_0^3}{\lambda} \sqrt{(B'_{11} - B'_{22})^2 + 4B'_{12}B'_{12}^*}. \tag{14}$$

The transmissions T_f and T_s in Eqs. (9) and (10) depend on the length l according to the formulae

$$T_f^2 = \exp(-\kappa_f l), \quad T_s^2 = \exp(-\kappa_s l), \quad (15)$$

where κ_f and κ_s are the length-independent absorption coefficients. The difference $\kappa_f - \kappa_s$ is related with the relative difference in transmissions

$$(T_f - T_s)/\bar{T} = 2 \tanh[-0.25(\kappa_f - \kappa_s)l], \quad (16)$$

where $\bar{T} = (T_f + T_s)/2$ is the average transmission coefficient. The absolute value $|(T_f - T_s)/\bar{T}|$ can be measured by the method outlined previously in Ref. [3]. The experimental value of $|(T_f - T_s)/\bar{T}|$ obtained for a given length l along with equation (16) allow us to find a value for any l . The other terms involving transmissions in Eq. (9) and (10) may be approximated as $T_f^2 + T_s^2 \approx 2\bar{T}^2$ and $T_f T_s \approx \bar{T}^2$, which allows for the reduction of \bar{T} in further calculations of the modulation index.

It is worth noting that according to Eqs. (9) and (10) the natural optical activity of the liquid sample can not be compensated by rotations of the analyzer and the optimal conditions for measurements of electro-optic coefficients occur only for $\alpha_a = -45^\circ$ and $+45^\circ$. Two possible orientations of the polarizer, two orientations of the analyzer and two for the quarter-wave plate give eight combinations, which lead to four nonequivalent results either in equation (9) or (10). Each of these cases corresponds to different perturbations in electro-optic measurements by other unintended effects occurring at the same time.

3. RESULTS OF NUMERICAL CALCULATIONS

In the case of solid crystals the influence of imperfect crystal cutting and alignment on the accuracy of the measurements of the quadratic electro-optic coefficients is one of the major experimental problems. However, this source of errors becomes of little importance when measurements are performed for liquids, where the optic axis in the liquid spontaneously orients perpendicular to the plane of the electrodes and the linear birefringence $|n_{01} - n_{03}|$ is several orders of magnitude smaller than in crystals. Very low linear birefringence enables, however, a stronger manifestation of the optical activity and dichroism, even in directions far from the optic axis.

Let us consider in more detail the measurements of the $q_{13} - q_{33}$ effective coefficient in the castor oil using a sinusoidal modulating field $E = E_0 \sin(\omega t)$, which is directed perpendicular to the light beam. We assume that experimental

data are typically processed employing the simplified formula that results from both Eqs. (9) and (10) for idealized conditions where the sample is isotropic ($n_{01} = n_{03}$), not dichroic ($T_f = T_s = T$), not optically active ($B'_{12} = 0$), and the phase difference Γ is so small that $\sin \Gamma \approx \Gamma$

$$|q_{13} - q_{33}| \approx \frac{2\lambda}{\pi l n_0^3} \frac{m_{2\omega}}{E_0^2}. \quad (17)$$

$m_{2\omega}$ in Eq. (17) is the modulation index defined as the ratio

$$m_{2\omega} = I_{2\omega} / I_0, \quad (18)$$

where I_0 is the constant component of the transmitted light intensity I , and $I_{2\omega}$ is the intensity at the second harmonic of modulating field. In our example the values of I_0 and $I_{2\omega}$ are calculated using the exact formulas presented in Chapter 2 by employing the form of the $[B']$ tensor for the $\infty 2$ symmetry given in Eq. (7).

We used the following values published previously for the castor oil at room temperature obtained at $\lambda = 632.8$ nm: $n_0 = 1.48$, $|n_{01} - n_{03}| \approx 1.6 \cdot 10^{-7}$, $g_{11}^{(0)} = 2.2 \cdot 10^{-7}$ and $|(T_f - T_s)/\bar{T}| = 0.036$ given for $l = 10$ cm [3]. The effective electro-optic coefficient $|q_{33} - q_{13}| = 2\lambda K/n_0^3 \approx 5.8 \cdot 10^{-21} \text{ m}^2\text{V}^{-2}$ was found by using the published value of the Kerr constant $K \approx 1.5 \cdot 10^{-14} \text{ mV}^{-2}$ measured in the fresh castor oil at temperature 297 K [1]. Currently, there is a lack of data in the literature concerning the electrogyration in liquids which are not liquid crystals. Our initial results, which are not published yet, show, however, that the β_{31} coefficient in the castor oil is of the order of $10^{-23} \text{ m}^2\text{V}^{-2}$. Thus the electrogyration effect is negligible when the quadratic electro-optic effect manifests itself at the same time.

Considering the impact of undesirable effects on measurements of the effective coefficient $g_{\text{ef}} = |q_{33} - q_{13}|$, we use the following relative error

$$\Delta \approx 100\% \cdot (g_{\text{ef}} - g_{\text{ef}}^{\text{id}}) / g_{\text{ef}}^{\text{id}}, \quad (19)$$

where g_{ef} is the inaccurate value determined from the simplified equation (17) and $g_{\text{ef}}^{\text{id}}$ is the ideal value, which is assumed in advance in our numerical analysis. The results of calculations presented in Fig. 1 show that the error Δ depends significantly on the light path-length l , and the dependences is clearly different for four nonequivalent combinations of the azimuths α_a , α_p and $\alpha_{\lambda/4}$. We would like to emphasise that the smallest values of l does not guarantee the smallest errors. This result is a consequence of two proportionalities $T_f^2 - T_s^2 \sim l$ and $\sin \Gamma \sim l$, which are satisfied for the smallest values of l , where the term $T_f^2 - T_s^2$ in Eqs. (9) and (10) is related to the factors that disturb the measurement, and the term $\sin \Gamma$ is related to the expected contribution of the

electro-optic effect to the modulation index m_{20} . The next important source of errors is related to the non-linearity of the term $\sin \Gamma$. Because of the linear and circular birefringence in the oil the constant part of Γ may reach the values for which the approximation $\sin(\Gamma) \approx \Gamma$ becomes insufficient for the length l of the order of centimetre.

Since the data $(T_f - T_s)/\bar{T}$, $n_{01} - n_{03}$, and $q_{33} - q_{13}$ are known only as absolute values, we can not assign the individual curves on Fig. 1 to the specific values of the azimuths α_a , α_p , and $\alpha_{\lambda/4}$. Regardless of the signs, we can always identify that pair of measurement series, for which the measurement errors are almost compensated in the results presented as the arithmetic mean of two series. A pair of suitable series are, for example, the series that differ in the azimuth of the quarter-wave $\alpha_{\lambda/4} = 0^\circ$ or 90° , while the orientation of other components are the same. Moreover, the results suitable for averaging can also be obtained for different azimuths α_a or α_p , with the same azimuth $\alpha_{\lambda/4}$. If the quarter-wave plate is placed between the polarizer and the cuvette, the suitable series should differ only in the azimuth $\alpha_p = -45^\circ$ and $+45^\circ$, and if the quarter-wave plate is placed between the cuvette and the analyzer the suitable series should differ only in $\alpha_a = -45^\circ$ and $+45^\circ$.

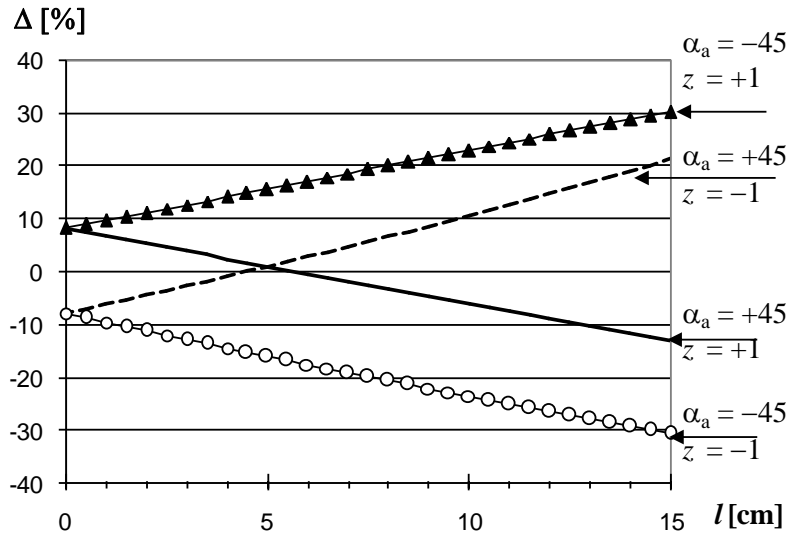


Fig. 1. The effect of the light path-length l on the relative error Δ [%] in the measurement of $|q_{13} - q_{33}|$ in the castor oil. The exemplary legend for the curves are given for the case when $\alpha_p = -45^\circ$, the sign of $(T_f - T_s)/\bar{T}$, $n_{01} - n_{03}$, and $q_{33} - q_{13}$ are positive, and the quarter-wave plate is placed behind the cuvette

4. CONCLUSIONS

The analysis presented in this work shows that the optical polarimetric method enables the measurements of electro-optic coefficients in optically active liquids, but the measurable coefficients depends on the symmetry of the sample of liquid. In the case of isotropic liquid with the $\infty\infty$ internal symmetry the effective coefficient $q_{11} - q_{12}$ of the quadratic electro-optic effect can be measured, which is equivalent to $q_{13} - q_{33}$.

The transition to the $\infty 2$ symmetry observed e.g. in the castor oil placed between plane-parallel electrodes is associated with the permission for the linear electro-optic and linear electro-gyration effects and with the inequality $q_{11} - q_{12} \neq q_{13} - q_{33}$ (see Tables 1 and 2). However, the both linear effects and the quadratic one described by $q_{11} - q_{12}$ cannot manifest themselves in the observed situation where the optic axis in the oil spontaneously orients in the direction perpendicular to the plane of the electrodes, and the only measurable coefficient is $q_{13} - q_{33}$. The deviation from the $\infty\infty$ symmetry observed in the castor oil may be higher or lower depending on many factors such as the electrode material, temperature, and the intensity of an applied electric field. Thus, it is possible that the value of the $q_{13} - q_{33}$ coefficient measured in a given sample may depend on measurement conditions.

In the case of the ∞ symmetry the linear electro-optic effect described by the $r_{13} - r_{33}$ coefficient should be strongly manifested in the optical response of the measurement system. Currently the linear response has been not observed in our measurements with liquids subjected to the sinusoidally varying field. Nevertheless, the ∞ symmetry should be reconsidered when the results for the static electric field would be available.

The example presented in Section 3 concerns the error analysis for the measurement of the effective quadratic electro-optic coefficient $|q_{13} - q_{33}|$ in the castor oil, which exhibits the symmetry $\infty 2$ between a pair of plane-parallel electrodes. The numerical results obtained show that the measurements performed using the optical polarimetric method are sensitive to the influence of some undesired effects, such as the dichroism, natural linear birefringence, and natural optical activity, while the activity induced by an applied electric field (electrogyration effect) seems to be negligible. The measurement error significantly depends on the path-length of the light in the oil, but the shortest lengths do not guarantee the smallest measurement error. The contribution of undesirable effects can be mostly reduced in the results presented as an arithmetic mean of the two measurement series, which differ e.g. in the orientation of the quarter-wave plate.

REFERENCES

- [1] **Stępień M., Ledzion R., Górski P., Kucharczyk W.**, Sci. Bull. of the Lodz University of Technology, s. Physics, **33** (2012) 89.
- [2] Castor oil for research purposes from Sigma-Aldrich, Specification Sheet, product number 259853 (available at www.sigmaaldrich.com).
- [3] **Izdebski M., Ledzion R., Górski P.**, Sci. Bull. of the Lodz University of Technology, s. Physics, **33** (2012) 39.
- [4] **Tomkins H.G., Irene E.A.**, Handbook of Ellipsometry, William Anderw, 2005, p. 121.
- [5] **Maldonado T.A., Gaylord T.K.**, Appl. Opt., **28** (1989) 2075.
- [6] **Sirotnin Yu.I., Shaskolskaya M.P.**, Fundamentals of crystal physics, Mir Publishers, 1982.
- [7] **Ścierański J., Ratajczyk F.**, Optik (Stuttgart), **68** (1984) 121.
- [8] **Izdebski M.**, J. Appl. Cryst., **45** (2012) 950.

ANALIZA POMIARU KWADRATOWEGO EFEKTU ELEKTROOPTYCZNEGO W OLEJU RYCYNOWYM

Streszczenie

Przedstawiono rozszerzoną teoretyczną analizę odpowiedzi układu pomiarowego na przyłożone pole elektryczne podczas pomiarów współczynników efektu elektrooptycznego w cieczy aktywnej optycznie metodą polaryzacyjno-optyczną. Analiza obejmuje ciecze o symetriach wewnętrznych opisanych grupami Curie $\infty\infty$, $\infty 2$ oraz ∞ i uwzględnia następujące zjawiska: naturalna aktywność optyczna, naturalna dwójłomność liniowa, dichroizm oraz efekty indukowane przez przyłożone pole elektryczne – liniowy i kwadratowy efekt elektrooptyczny oraz liniowa i kwadratowa elektrozyracja. Przedstawiony przykład dotyczy numerycznej analizy błędu pomiaru kwadratowego efektu elektrooptycznego w oleju rycynowym, który wykazuje symetrię $\infty 2$ po umieszczeniu go pomiędzy płasko-równoległymi elektrodami.

SYLWESTER KANIA^{1,2}

¹Institute of Physics, Lodz University of Technology

ul. Wólczańska 219, 90-924, Łódź, Poland

²Centre of Mathematics and Physics, Lodz University of Technology

Al. Politechniki 11, 90-924 Łódź, Poland

HOLE DRIFT MOBILITY FOR DIFFERENT STRUCTURES OF ANTHRONE AND ANTRACHINONE LAYERS

Drift mobility of holes in antrachinone and anthrone thin films evaporated in the vacuum of the order of 10^{-5} Tr was determined with time of flight method (TOF). The layers had different structural order due to the temperature of vaporized substrates. The results show almost lack of the mobility dependence due to the structural order. One order of difference in mobility values for antrachinone and anthrone may have origin in the presence of the difference in permanent dipole moment of the molecules.

Keywords: polycrystalline films, quasi amorphous films, amorphous films, anthrone, antrachinone, hole drift mobility, carrier transport.

1. INTRODUCTION

The paper concern the problem of the origin of the differences in the hole transport for the thin layers of acenes. For this reason we have studied layers with different crystal order, that is polycrystalline, quasi-amorphous and amorphous for two compounds with different molecular dipole moment but with nearly identical crystalline structure, that is for antrachinone and anthrone.

Antrachinone and anthrone are the promising materials for thin layer organic electronics. The organic layers are the compromise between strong

coupling forces in the molecule in the sense of the covalent bonds and intermolecular forces dependent on the weak hydrogen or van der Waals bonds in the range of 10^{-3} - $7 \cdot 10^{-2}$ eV. The energy of the dipol-dipol interactions between molecules with permanent dipole moment is with some approximation described by the formula:

$$U_{d-d} = -\frac{2c}{3kT} \frac{\mu_a^2 \mu_b^2}{r^6}$$

where r – is a distance between centres of dipoles, μ – dipole moment, k – Boltzmann constant ($1,38 \cdot 10^{-23}$ JK⁻¹) and T – thermodynamic temperature.

In the case of anthraquinone molecules with natural dipole moment measured in benzene of 0,6 D ($2,00 \cdot 10^{-30}$ Cm) [1], this energy is in the order of 10^{-5} - 10^{-6} eV, what does mean three orders of magnitude less than the van der Waals potential. Anthrone molecules possess a greater natural dipole moment, which for example when measured in benzene is of 3,66 D ($1,22 \cdot 10^{-29}$ Cm) [1] and the energy of dipol-dipol interaction can be estimated in the order of 10^{-2} - 10^{-3} eV, comparable to the van der Waals potential. The additional dipol-dipol energy present for anthrone structures can lead to broadening of the bands in the case of layer of ordered state, or can lead to the higher overlapping of the wave functions for the charge carriers conducting via localized states.

2. EXPERIMENTAL AND RESULTS

2.1. Properties of anthraquinone and anthrone

The structures of anthraquinone, C₁₄H₈O₂, and anthrone, C₁₄H₁₀O are nearly the same, monoclinic with space group C_{2h}⁵(P2₁/a) with bimolecular unit of the dimensions (at room temperature) $a_0 = 15,8$ Å, $b_0 = 3,94 - 3,99$ Å, $c_0 = 7,865(10)$ Å, $\beta = 102^\circ 43(2)'$ for anthraquinone, and $a_0 = (15.80 \pm 0.03)$ Å, $b_0 = (3.998 \pm 0.005)$ Å, $c_0 = (7.86 \pm 0.16)$ Å, $\beta = 101^\circ 40'$ for anthrone [2, 3]. The main difference essential for the reason of this paper is the fact that the anthraquinone molecules posses negligible dipole moment, opposite to the anthrone molecules which are characterised by large dipole moment of 3,6 D.

2.2. Sample preparation

The spectral grade anthraquinone and anthrone (purified with zone melting) were used for obtaining thin film samples by evaporation in vacuum under the pressure of the order of 10^{-5} Torr on glass plates supplied with gold electrode.

The substrates temperatures during evaporation for polycrystalline layers were kept near 300 K, and for quasi amorphous layers were kept in the range of 170-200 K using a proper evaporation rate. Structural examination of the antrachinone and anthrone layers were made using automatic X-ray diffractometer DAR [4, 5]. The exemplary X-diffractograms are presented in Figs. 1 and 2.

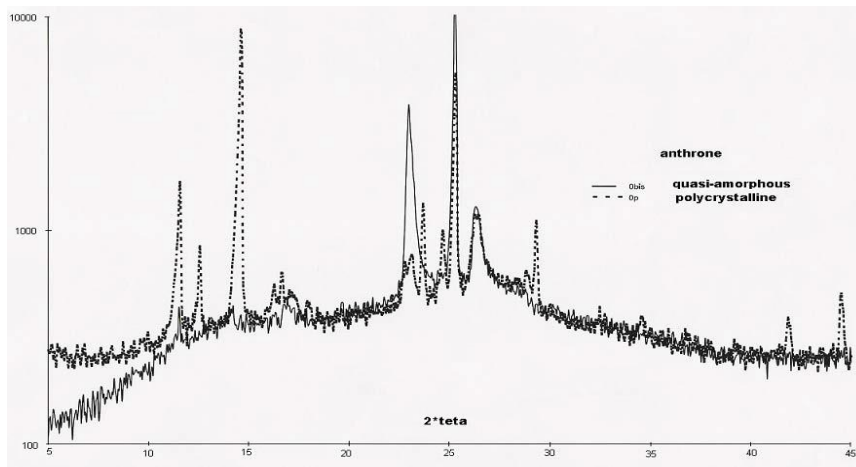


Fig. 1. Diffraction pattern (X ray) for polycrystalline and quasi-amorphous anthrone layers

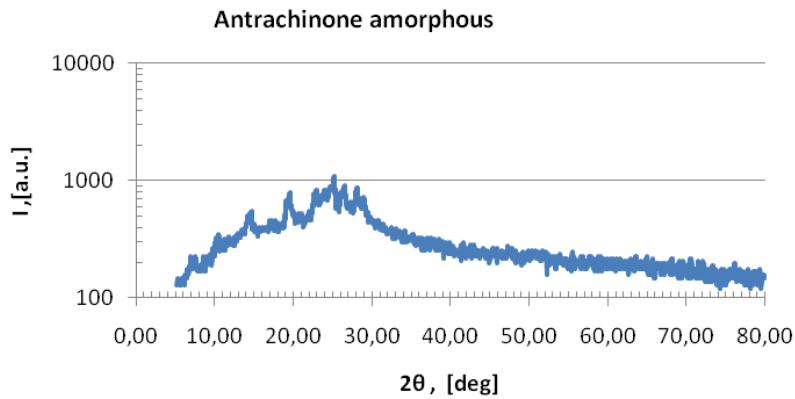


Fig. 2. Diffraction pattern (X-ray) for amorphous antrachinone layers

2.3. Measurements

Free pairs of electron-hole were generated by a nitrogen laser, with the pulse intensity of $5 \mu\text{J}$ and with pulse duration width $t_{1/2}$ of 8 ns. Measurements were made using the time of flight set-up working under computer control which enables to control the measurements and to store the data. The time of flight was found from the current signal. The current pulses were measured with digital oscilloscope Hung Chang DSO 5804 and Rigol DS1062CA. The system details were completely described in [6,7]. The examinations of the hole mobility for the polycrystalline anthracene layers were made at the room temperature biasing with the electrical field in the limits from $3 \cdot 10^3 \text{ V/cm}$ to $2 \cdot 10^4 \text{ V/cm}$. The determination of the activation energy of the mobility for these layers was made in the temperature limits 285-353 K.

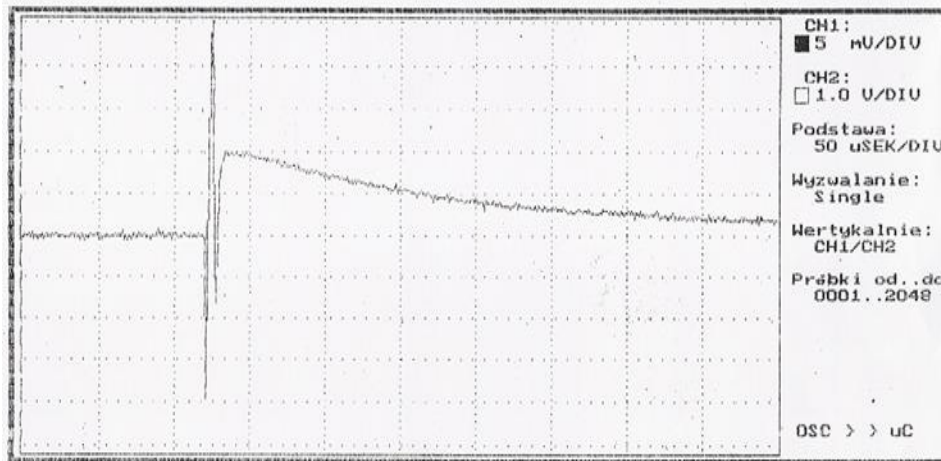


Fig. 3. Typical current pulse for amorphous anthrone layers

The examinations of the hole mobility for the polycrystalline anthrone layers were made in the limits of the electrical field from $1 \cdot 10^3 \text{ V/cm}$ to $2 \cdot 10^4 \text{ V/cm}$. Measurements for amorphous and quasi amorphous anthrone and anthracene were made in the limits from $1 \cdot 10^3 \text{ V/cm}$ to $1 \cdot 10^4 \text{ V/cm}$. All the measurements were made at room temperature. The activation energy of mobility for those layers was determined in the temperature limits 285-353 K. Typical current pulse obtained for the amorphous anthrone layers is presented in Fig. 3. The values of the electric fields applied in the time of flight measurements have been chosen after taking the U - V characteristics for which

we had obtained the level when the traps were fulfilled. For this and greater values of the field we have obtained the shape of the pulse which possessed the “kink point” on the $I-t$ characteristics plotted in the log-log scale.

2.4. Results

For the polycrystalline layers of antrachinone and anthrone the mobilities for holes were in the range $(8\pm 2)\cdot 10^{-4}$ cm²/Vs and $(7\pm 2)\cdot 10^{-3}$ cm²/Vs. Temperature dependences of the mobility μ in cm²/Vs were given by formulae

$$\ln \mu = -\frac{3365}{T} - 3,643$$

for antrachinone and

$$\ln \mu = -\frac{3896}{T} - 5,622$$

for anthrone polycrystalline layers. These results indicate the activation energy of the order 0,03 eV, which is close to kT (0,026 eV). Additionally the shape of those dependences presented in log-log scale with “kink point” may approve the assumption that the hopping transport is present in the layers for both studied materials and that the activation energy for hopping is of the order of 0,03 eV [8, 9].

The measurements of the hole mobility were made within limits of the electrical field from $1\cdot 10^3$ V/cm to $1\cdot 10^5$ V/cm. The investigations were made in the room temperature and the results are presented in the Table 1.

Table 1

compound	ordering	hole mobility μ [cm ² /Vs] ($T = 300$ K)	activation energy E_a [eV]	applied electric field [V/cm]
antrachinone	polycrystalline	$(8 \pm 2)\cdot 10^{-4}$	0,03	$3\cdot 10^3$ to $2\cdot 10^4$
antrachinone	quasi-amorphous	$(3-7)\cdot 10^{-4}$	0,03	$3\cdot 10^3$ to $2\cdot 10^4$
antrachinone	amorphous	$(0,9-6,0)\cdot 10^{-4}$	0,03	$3\cdot 10^3$ to $2\cdot 10^4$
anthrone	polycrystalline	$(7\pm 2)\cdot 10^{-3}$	0,03	$1\cdot 10^3$ to $1\cdot 10^5$
anthrone	quasi-amorphous	$(3-7)\cdot 10^{-3}$	0,03	$1\cdot 10^3$ to $1\cdot 10^5$
anthrone	amorphous	$(0,6-4,0)\cdot 10^{-3}$	0,03	$1\cdot 10^3$ to $1\cdot 10^5$

For both molecular crystals the values of the mobility are below 10^{-2} cm²/Vs, and the estimated values of the activation energy are the same.

Despite of almost the same crystallization structure (the space group $C_{2h}^5(P2_1/a)$ operates for both), clear differences in the magnitude of mobility were observed. For anthrone, with molecule possessing a natural dipole moment,

the mobility of holes in the condensed state is almost one order of magnitude greater than that measured for anthracinone.

3. CONCLUSIONS

Findings of investigations demonstrate that the conductivity of both exercised spectral grade compounds does not exhibit the explicit dependence on the structure of the layer. For the anthracinone layers with perturbed crystal order, the value of holes mobility was smaller than $1 \cdot 10^{-3} \text{ cm}^2/\text{Vs}$ at room temperature, which is typical for acenes, whereas for anthrone layers the mobility of the holes was almost one order of magnitude greater.

Measurements of the drift mobility in the discussed range of temperature for both of the acenes gives nearly identical character of the temperature dependence of this mobility, $\mu_d = \mu(T)$. In the range of error, it has an activated character with small activation energy of the order of kT .

The methodology of the experiment excludes influence of coordination of the molecule and influence of short-range and long-range ordering on observed differences in the conductivity for both compounds. Therefore the differences in the measured mobility may be attributed to the differences in permanent dipole moment for both examined molecules.

The carrier mobility values and activation energy suggest that we can meet here with two possibilities: the band transport with participation of traps [10] or with hopping transport [10, 11]. The more precise determination needs further studies on the influence of the structural disorder on the mobility value.

Acknowledgements

Great thanks to prof. B. Marciniak and prof. M. Wieczorek for preparation of the spectral grade anthracinone and anthrone and for enabling the Roentgen analysis and to prof. J. Świątek for valuable discussions.

REFERENCES

- [1] Weber G., Z. Naturforsch. B, **36** (1981) 896.
- [2] Kania S., Kondrasiuk J., Bąk G. W., Eur. Phys. J. E, **15** (2004) 439.
- [3] Landolt-Börnstein, Zahlenwerte und Funktionen aus Naturwissenschaften und Technik, Springer Verlag, Berlin, 1971.
- [4] Kania S., Sci. Bull. Tech. Univ. o Łódź, s. Physics, **28** (2007) 27.

- [5] **Kania S.**, Sci. Bull. Tech. Univ. of Łódź, s. Physics, **30** (2009) 65.
[6] **Kania S., Kondrasiuk J.**, Sci. Bull. Tech. Univ. of Łódź, s. Physics, **23** (2003) 25.
[7] **Kania S.**, Visnyk of Lviv Univ., Series Physical, **43** (2009) 49.
[8] **Silinsh E., Čapek V.**, Organic molecular crystals, AIP Press, New York, 1994.
[9] **Kania S.**, Sci. Bull. Tech. Univ. of Łódź, s. Physics, **33** (2012) 56.
[10] **Mott N. F., Davies E. A.**, Electronic Processes in Non-Crystalline Materials, Clarendon Press, Oxford, 1971.
[11] **Mycielski W.**, J. Non-Crystalline Solids, **37** (1980) 267.

DRYFTOWA RUCHLIWOŚĆ DZIUR W WARSTWACH ANTRONU I ANTRACHINONU O RÓŻNEJ STRUKTURZE

Streszczenie

Badano proces transportu dziur w polikrystalicznych, quasi-amorficznych i amorficznych warstwach antronu i antrachinonu. Do naparowania warstw w próżni 10^{-5} Torr użyto materiałów o czystości spektralnej. Pomiary ruchliwości wykonano metodą TOF. Obydwa związki z punktu widzenia krystalograficznego posiadają prawie jednakową strukturę układu jednoskośnego o prawie identycznych stałych sieciowych i prawie identycznym kącie β . Przebadano trzy rodzaje warstw, to jest o strukturze polikrystalicznej, quasi-amorficznej i amorficznej. Dla warstw antronu, którego cząsteczki posiadają stały moment dipolowy, uzyskano prawie o rząd większą wartość ruchliwości niż dla warstw antrachinonu, niezależnie od stopnia uporządkowania tych warstw. Dla obu związków uzyskano w temperaturze pokojowej wartości ruchliwości mniejsze niż 10^{-2} cm²/Vs z energią aktywacji ruchliwości rzędu 0.03 eV. Uzyskane wartości przemawiają za transportem hoppingowym. Na podstawie badań wydaje się, że moment dipolowy cząsteczek może mieć istotny wpływ na wielkość ruchliwości nośników ładunku.

SYLWESTER KANIA^{1,2}, JANUSZ KULIŃSKI²¹Institute of Physics, Lodz University of Technology
ul. Wólczańska 219, 90-924, Łódź, Poland²Centre of Mathematics and Physics, Lodz University of Technology
Al. Politechniki 11, 90-924 Łódź, Poland

ADSORPTION OF ETHANOL TO THIN LAYER OF ACENES AS A PROCESS OF INTERCONNECTED NETWORKS

The activation process and the transport process for electrons in the tetracene layers and holes in the p-quaterphenyl layers is considered. Observed dependence of the conductivity on the vapor concentration of the activator molecules may suggests influence of collisions as a source of injection of charge through the surface potential barrier of adsorption. Applied model of two-body interactions in the interface of adsorption is approved on the basis of theory of area law for entanglement from exponential decay of correlations. Quantum description of adsorption of small hydrocarbon to the solid acenes involve only diagonal elements of the interaction matrix.

Keywords: tetracene films, p-quaterphenyl films, adsorption, interconnected networks.

1. INTRODUCTION

Organic semiconductor gas sensors are very appropriate for vapour detection, because they change their conductivity when exposed to vapours. The changes can be correlated quantitatively to the vapours concentration. The interactions of the gas molecules with organic layer can be considered as a kind of injection of the carriers.

This work explores the influence of the adsorption of the volatile ethanol molecules to the surface of polycrystalline tetracene or p-quaterphenyl. The electrical response measured when the layer is exposed to ethanol vapour shows

a deep decrease of the resistance of the film. We have noticed that the presented sensor layers exhibits attractive performances, good sensitivity to the ethanol, deep modulation of the current up to current density of 10^{-5} A/cm². These features suggest possibility of some application. In this paper we try to describe and explain some processes related to the structure of the surface with contact of the vaporized ethanol. We also try to describe the features present in the layer in dependence on the charge transfer through the surface layer. We employ the concept of the quantum transition theory matched with the model of interconnected networks. For this reason, the Hamiltonian was constructed, which takes into account the particles interacted with solid surface originated from gas in the ensemble of the adsorbing layer as well as the ensemble of interacting skin layer of the solid. The Hamiltonian obtained in the course of such description ought to be noticed as the sum of the terms for two-particle interactions. Such interpretation leads to the model of independent conductivity channels.

2. EXPERIMENTAL

Thin films of tetracene (C₁₈H₁₂) and of p-quaterphenyl (C₂₄H₁₈) made as a sample of "sandwich" type with Au – Al electrodes were prepared with vacuum deposition method. The polycrystalline samples were obtained by evaporation in vacuum under the pressure of the order of 10^{-5} Torr on glass plates covered with metal film. The substrate temperature was about 300 K and the evaporation rate was changed in the range 20-30 Å/s. Structural examination of the obtained layers was made using X-ray diffraction with an automatic diffractometer DAR. Diffraction studies were made in the 2θ range from 5° to 80° with measuring step 0.05°. Experimental setup [1,2] consisted of the current source and electronic recorder and allowed to take measurements and registration of changes of a dark current flow through the sample during the action of activator. Once the system was vaporized with ethanol, the current continued to increase and it saturated between every step of vaporization. The kinetics of the current for tetracene and p-quaterphenyl films vaporized with C₂H₅OH are presented in Fig. 1.

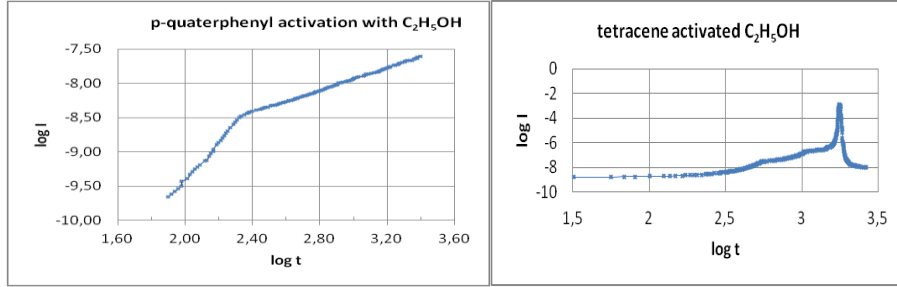


Fig. 1. Kinetics of the current for tetracene and p-quatephenyl films vaporized with C_2H_5OH

3. MODEL

In previous papers we have recognised conduction due to the absorption of the ethanol to the tetracene or p-quatephenyl as the variety of the transition state reactions [3, 4]. If we want to describe dynamic properties of adsorption layer in interaction with surface we must separate the thermodynamic subsystem of interacting molecules [5,6] and determine the directivity of interactions. In the papers [6-8], we have characterized the phenomenological structural model of the interacting surface and we have developed a perturbed Hamiltonian for such system. The important feature of quantum many-body states is amount of entanglements in the state. Taking into account the fact that the adsorption layer decay in the conditions of vacuum may have width of few angstroms we can adopt the theory of an area law for entanglement from exponential decay of correlations [9]. In the scope of this model using the second quantization for a given bipartite-mixed quantum state ρ_{XY} , we can quantify the correlation between X and Y. Correlation function generalizes two point correlation functions, in the condensed-matter physics, in which both X and Y are composed of a single sites, (Fig. 2). In accordance with the concept of abrupt transition in the structural formation of interconnected networks [9,10] we can apply this model to the gas molecules in the adsorption layer as well as to the nodes in the solid surface. The quantum state $|\psi\rangle_{1,\dots,n}$ composed of n qubits defined on a finite dimensional lattice has ξ -exponential decay of correlations if for every two regions X and Y separated by l sites

$$Cor(X : Y) \leq 2^{-l/\xi} \quad (1)$$

Here ξ – is the correlation length of the state.

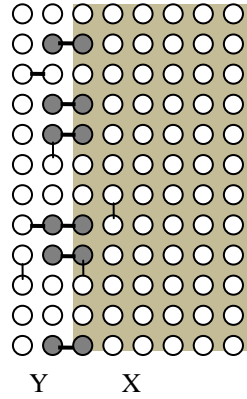


Fig. 2. Model of adsorption layer as a system of entangled pairs X and Y. Shaded square denotes region of solid layer. Pairs crossing the boundary (dark) contribute to the entropy of the region inside the layer [7]

Tetracene and p-quaterphenyl molecules have length between 12 and 16 Å, and the molecules of activator - ethanol are 8-10 times shorter. Aromatic rings act as hydrogen bond acceptors [11], with bonding proton at a distance of 1 Å from the centre of benzene ring, and the total length of the hydrogen bond does not exceed 4,2 Å. In the reason of the model of adsorption layer as a system of entangled pairs (see the Fig. 2), we can estimate l as 12 Å, and ξ as 4,2 Å, then from equation (1) we can obtain:

$$Cor(X : Y) \leq 2^{-4,2/12} = 0,785$$

This result confirms the assumption of low width of the adsorption layer and gives entanglement E of X and Y (in our case: ethanol - solid layer) as a function of reduced density matrix of $|\psi\rangle_{X,Y}$ dependent only on one of the regions, for example X. Obtained in this manner von Neumann entropy H is proportional to its boundary not to the volume of the system [9]:

$$E(|\psi\rangle_{XY}) = H(\rho_X) = -tr(\rho_X \cdot \log \rho_X) \quad (2)$$

where ρ_X is the reduced density matrix of $|\psi\rangle_{XY}$ on the region X.

There can be underlined the fact that the value of correlation we have obtained is without any assumptions about the shape of the potential. In [9], the theorem is proven, that such model can be applied to the disordered Hamiltonians exhibiting many-body localization or mobility gap always fulfill an area law. In our case we have constant area of active nodes in the surface layer (all surface molecules are made of benzene rings) and if we recognize them as a X sites in equation (2) then in the scope of this model a description using the

Hamiltonian in the manner of sum of terms centered on the active nodes is approved. This leads to the conclusion that simple Schrödinger equation in the manner presented in [6] with potential centered on the lattice rings: $V_{ij}(x_i, y_j, r)$ [4] (where x_i and y_j denote the surface coordinates of the absorbing ring), and with $U_{k,k'}$ – interaction potential between different gas molecules (numbered by k) in the absorbing layer, V_{ck} – the potential centered on the absorbing molecule and U_k – potential energy of the absorbing particles in the absorbing layer is good approximation for adsorption of shorter molecules of ethanol at the rings of acenes. The Schrödinger equation will be of the shape:

$$H\psi = \left[-\frac{\hbar^2}{2m} \sum_{i,j} \Delta_{i,j} + \sum_{i,j} V_{i,j}(x_i, y_j, r_k) + \sum_{i,j} (V_{ck})_{i,j} + \sum_k U_k + \sum_{k,k'} U_{k,k'} \right] \psi \quad (3)$$

where $\Delta_{i,j} = \partial^2/\partial x_i^2 + \partial^2/\partial y_j^2$.

On the basis of the theory considered above, the solution may be given as the linear combination of the electron wave function ψ_k of the adsorbate gas and rings of the solid layer $\psi_{i,j}$:

$$\psi_{i,j} = a_{k,i,j} \psi_k + \sum_{i,j} a_{i,j} \psi_{i,j} \quad (4)$$

where: $|a_{k,i,j}|^2$ denotes the probability to find the electron on the k -th absorbing molecule, and $|a_{i,j}|^2$ denotes the probability to find the electron at the i,j -th ring. The correlation value we have obtained above in the scope of model of abrupt transitions in structural formation of interconnected networks approve reduction of this wave function to the function centered only on layer rings (or equivalently on the nodes of the (imagine) network made for adsorbing gas molecules:

$$\psi_{i,j} = a_k \psi_k + a_{i,j} \psi_{i,j} \quad (5)$$

If we separate problem to the sum of the terms centered on the each of k -th adsorbate particle then the result may approve the concept of multichannel mechanism of conduction in the region of the layer of adsorption. What more, with such boundary conditions, the problem of the transport inside the layer can be treated as a sum of the transported carriers originated from different kind of absorbing species permeating number of interconnected networks [10].

3. CONCLUSIONS

1. The kinetics of conductivity obtained during ethanol adsorption to the tetracene and p-quaterphenyl films are in coincidence with the two body collision mechanism.
2. Theorem of area interactions on the basis of theory of entanglement from exponential decay of correlations approved the picture with Hamiltonian described as a sum of interactions. The wave functions can be centered only at the nodes of one of interacting phases.
3. Modulation conductivity is probably connected with surface activation not with the diffusion of ethanol inside the layer.

ACKNOWLEDGEMENTS

Great thanks to prof. B. Marciniak and prof. M. Wieczorek for preparation of the spectral grade anthracinone and anthrone and for enabling the Roentgen analysis, and to prof. J. Świątek for valuable discussions.

REFERENCES

- [1] **Kania S.**, Sci. Bull. Technical University of Lodz, Physics, **22** (2002) 31.
- [2] **Kania S., Kondrasiuk J., Bąk G.W.**, Eur. Phys. J. E., **15**, (2004) 439.
- [3] **Kania S., Kuliński J.**, Chem. Met. Alloys, **4** (2011) 31.
- [4] **Kania S., Kuliński J.**, Sci. Bull. Lodz University of Technology, Physics, **33** (2012) 65.
- [5] **Kania S., Kuliński J.**, Sci. Bull. Technical University of Lodz, Physics **32**, (2011) 23.
- [6] **Velasco-Velez J. J., Kunze U., Haas T.**, Phys. Status Solidi A., **207** (2010) 924.
- [7] **Kania S., Kuliński J.**, Sci. Bull. Technical University of Lodz, Physics, **30** (2009) 47.
- [8] **Kania S., Kuliński J.**, Sci. Bull. Technical University of Lodz, Physics, **29** (2008) 45.
- [9] **Brandão F.G.S.L. and Horodecki M.**, Nature Phys., Vol. **9**, 11 (2013) 721.
- [10] **Radicchi F., Arenas A.**, Nature Phys., **9**, (2013) 717.
- [11] **Levitt M., Perutz M. F.**, J. Mol. Biol., **201** (1988) 751.

ADSORPCJA ETANOLU DO CIENKICH WARSTW ACENÓW JAKO PROCES WZAJEMNEGO ODDZIAŁYWANIA SIECI

Streszczenie

Badano proces aktywacji i proces transportu elektronów w warstwach tetracenu i p-kwaternofenu. Zależność procesów przewodnictwa od chwilowej wartości stężenia par aktywatora sugeruje wzrost natężenia prądu związanego z adsorpcją jako wynik procesów dwuciałowych zderzeń z wstrzykiwaniem nośników ładunku do warstwy. Słuszność takiego modelu uzasadnia twierdzenie o powierzchniowym charakterze oddziaływań wynikającym z teorii eksponencjalnego zaniku korelacji [9]. Teoretyczna analiza procesu adsorpcji węglowodoru na powierzchni pierścieniowego acenu nie wymaga znajomości wyrazów mieszanych macierzy przejścia. Powinno to prowadzić do znacznego uproszczenia procedury obliczania parametrów modelu oddziaływań.

**SYLWESTER KANIA^{1,2}, JANUSZ KULIŃSKI²
BERNARD MARCINIAK³, EWA RÓŻYCKA-SOKOŁOWSKA³**

¹Institute of Physics, Lodz University of Technology
ul. Wólczajska 219, 90-924, Łódź, Poland

²Centre of Mathematics and Physics, Lodz University of Technology
Al. Politechniki 11, 90-924 Łódź, Poland

³The Faculty of Mathematics and Natural Sciences
Jan Długosz University in Częstochowa
Al. Armii Krajowej 13/15, 42-218 Częstochowa, Poland

SOME ELECTRICAL PROPERTIES OF THIN LAYERS OF 9,10-DIMETHYLANTHRACENE AND 1-ACENAPHTHENOL

Spectral grade materials obtained in zone-melting process from commercially available 1-acenaphthenol and 9,10-dimethylanthracene were characterized electrically. The layers vaporized in 10^{-5} Torr vacuum possess high resistivity of the order of 10^{11} - 10^{12} Ωm and the concentration of traps lower than 10^{15} cm^{-3} .

Keywords: 1-acenaphthenol, 9,10-dimethylanthracene, conductivity, electric characterization.

1. INTRODUCTION

Organic molecular crystals in the type of thin films and aggregates are technologically very attractive materials in the electronic meaning. Their usefulness relies to a large extent on their photoconductivity, light absorption, non linear polarizability etc., which are significant for the properties immediately related to the electronic structure of these materials. Polycyclic aromatic hydrocarbons (PAH) has received much attention since optoelectronics needs materials with high grade of purity. Efficient charge transport requires that

the charges be able to move from molecule to molecule and not be trapped or scattered. The well known 1-acenaphthenol and 9,10-dimethylantracene (Fig. 1) are the promising materials for technology connected with organic electronics. But their structure was not described faultlessly till the last decade [2]. Commercially available ex-coal tar for acenes contains impurities in the order of 1% . For example for tetracene the typical representative compound of the semiconducting or photoconducting class, even low, e.g. $\leq 10^{-6}$ mol/mol [6] concentrations of the contaminations can essentially deteriorate the performance of mobilities for holes or for electrons, generating structural defects for trapping or scattering of chemical nature.

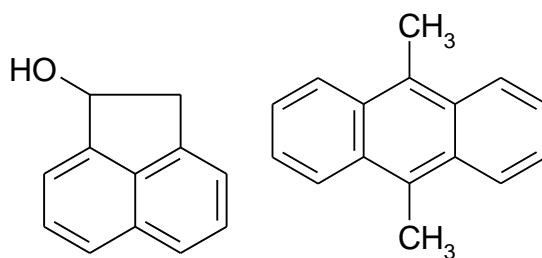


Fig. 1. Structures of 1-acenaphthenol and 9,10-dimethylantracene

2. EXPERIMENTAL AND RESULTS

During last decade, procedure for obtaining 9,10-dimethylantracene and 1-acenaphthol of sufficient purity grade for practical applications was developed [1-5]. This task was difficult. For example twenty one compounds and 14 impurities were identified in the commercially available [4] ex-coal tar acenaphthene and pyrene, respectively, with the help of Hewlett-Packard gas chromatographs type 6890 GC System and 5890 series II equipped with fused silica capillary columns and the FID and MS detectors. The naphthalene, 2-methylnaphthalene and 9H-fluorene, and 7-methylantracene, 1-phenylnaphthalene, fluoranthene and unknown compound with the molecular weight of 208 may be treated as the major impurities of the above hydrocarbons, respectively. The segregation coefficients of all the remaining detected

impurities with the exception of methyl dibenzofuran were lower than unity. This fact enabled to use the zone melting method for purifying. Impurities present in commercially available naphthalene, fluoranthene and anthracene have been concentrated by zone melting and further evaporation of their extracts in chloroform, and then they were identified by gas chromatography performed on CGC-FID and CGC-MS apparatuses. Quantitative contents of fourteen, eight and twelve impurities detected in naphthalene, fluoranthene and anthracene, respectively, have also been determined [3].

Purities of the obtained compounds were of the order of 99.999 mass% from which high quality crystals were grown. In order to characterize the intrinsic structure perfection of such grown crystals the X-ray examinations have been performed. The observed morphologies of these crystals have been compared with that predicted from PBC theory by Hartman-Perdok model growth conditions (vacuum, temperature gradient) effect have been assessed [1,4].

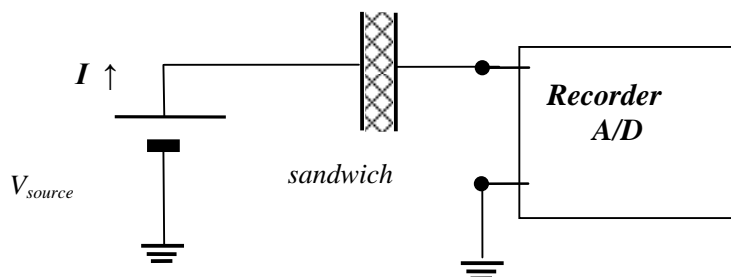


Fig. 2. Measuring setup for determination of $U-I$ characteristic

The purity of initial compounds used in experiments for this article was in the grade of 99.999 mass%. The layers of 1-acenaphthenol and 9,10-dimethylantracene were evaporated in the vacuum of order 10^{-5} Torr on the quartz glass plate supplied with Au electrode. On the top of the sandwich the aluminum electrode was evaporated. Such a structure has properties of plate condenser with the layer of dielectric. For such layers the capacitance was measured with Semi-Automatic RLC Bridge type E314. The width of the layers was evaluated from the capacitance and geometric dimensions of electrodes. Measured layers had the widths in the limits of 16-41 μm for 1-acephthenol and for 9,10-dimethylantracene.

Electrical characterization, in the form of $U-I$ characteristics, were made in the Faraday Cage supplied with a quartz window. Current-voltage characteristics were obtained for the field strength from $E = 2 \cdot 10^5$ to $2 \cdot 10^7$ V/m.

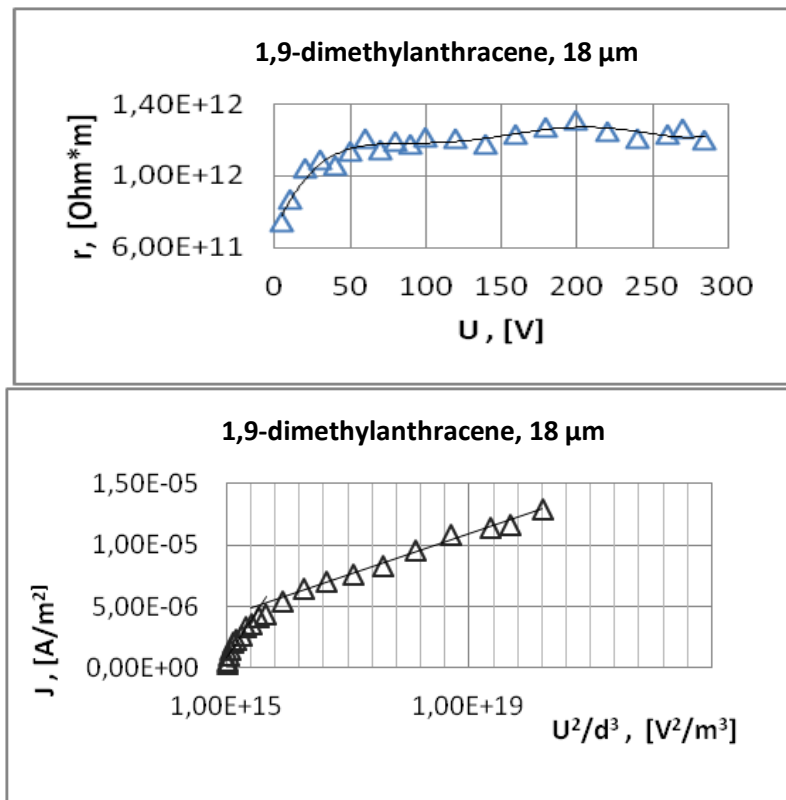


Fig. 3. Resistivity r as a function of voltage and current density J as a function of U^2/d^3 for 1,9-dimethylantracene, $d = 18 \mu\text{m}$

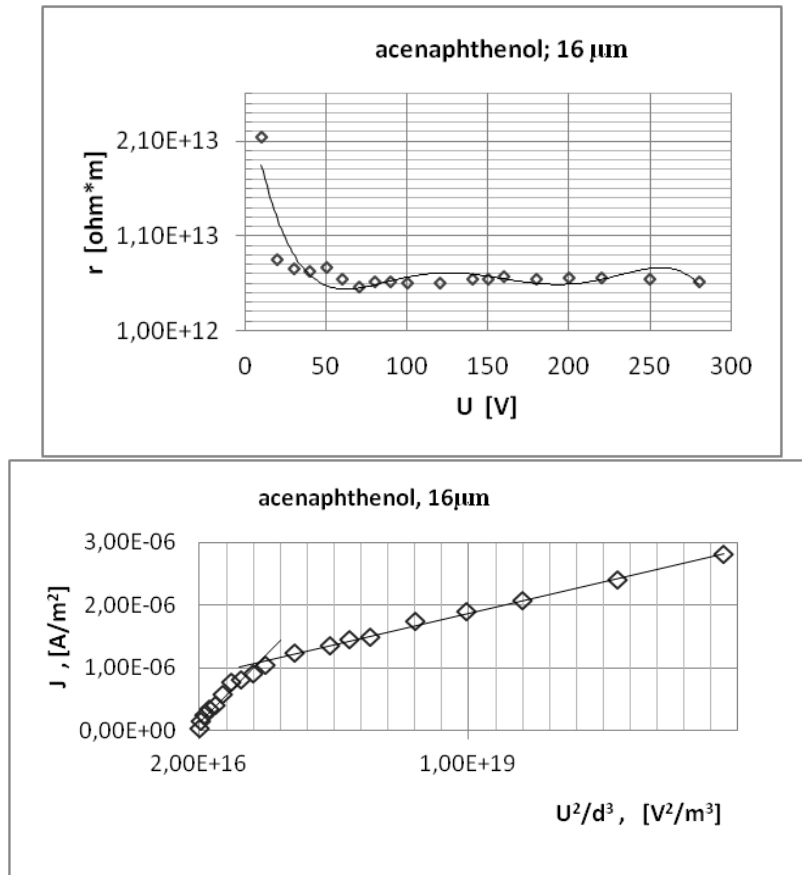


Fig. 4. Resistivity r as a function of voltage and current density J as a function of U^2/d^3 for 1-acenaphthenol, $d = 16 \mu\text{m}$

The data obtained for current-voltage characteristics are presented in Table 1.

Table 1

No.	compound	resistivity [Ω m]	conductivity [$S\ m^{-1}$]
1	1-acenaphthenol	$1.0 \cdot 10^{11} - 9.0 \cdot 10^{12}$	$1.1 \cdot 10^{-13} - 1.0 \cdot 10^{-11}$
2	9,10-dimethylantracene	$6 \cdot 10^{11} - 1.4 \cdot 10^{12}$	$7.1 \cdot 10^{-13} - 1.7 \cdot 10^{-12}$

The current flow through the thin dielectric layer of the thickness d , forced by the applied voltage, can be described by the known formula [8]:

$$J = \frac{9}{8} \varepsilon_0 \mu \mathcal{G} \frac{V^2}{d^3}$$

where μ is the mobility of the charge carriers and V is the voltage applied to the sample.

If only shallow traps occur in the studied dielectric then

$$\mathcal{G}(T) = n/n_t$$

where n is the total density of free charge carriers and n_t is the density of the trapped carriers. Those dependences are valid in the limits of the foundation of the bound model of transport with the shallow traps localized in the forbidden gap. Density of trapped carriers can be estimated from the intersection of two lines approximating two domains of J vs U^2/d^3 dependence in the manner presented in Figs. 3 and 4. This intersection points out the value of voltage for which the traps are filled. From this intersection point it was possible to determine the concentration of the traps. For 1-acenaphthenol layers the valuation gives the quantity in the limits $2 \cdot 10^{11} - 1 \cdot 10^{14}\ \text{cm}^{-3}$, and for the 1,9-dimethylantracene layers the value of $9 \cdot 10^{14}\ \text{cm}^{-3}$.

3. CONCLUSIONS

The layers of spectral grade compounds of 1-acenaphthol and 1,9-dimethylantracene are characterized with very high resistivity up to the electric field of $2 \cdot 10^7\ \text{V/m}$. Such great value can be attributed to lack of the double bonds in the ligands and to the herringbone structure not favorable the conduction.

Stabilization of the resistivity level is observed for the fields between $2 \cdot 10^6$ V/m and $2 \cdot 10^7$ V/m.

In the available measuring range the obtained resistivities of the examined layers were in the range $1,0 \cdot 10^{11}$ - $9,0 \cdot 10^{12}$ Ωm for 1-acenaphthenol and in the range of $6 \cdot 10^{11}$ - $1,4 \cdot 10^{12}$ Ωm for 9,10-dimethylantracene. The same field limits as for domains of stable resistivity were valid for linear higher voltage part of the diagram J vs U^2/d^3 . The domain seen in this diagram indicated the conditions of conductivity with fulfilled traps. Observed absence of other linear domains for higher voltages vote for existence of only one shallow trap state or only one shallow narrow band of traps. Such behaviour is valid for high purity grade organic materials. The data confirm the stability of these compounds in the conditions of thermal vaporization in the vacuum and their ability to nucleation layers on the gold electrodes without additional defects. Such materials can be used in the synthesis for obtaining more complicated organic materials for organic electronics [8].

REFERENCES

- [1] **Marciniak B., Różycka-Sokolowska E., Pawliuk W.**, Proc. SPIE, **4413**, International Conference on Solid State Crystals 2000: Epilayers and Heterostructures in Optoelectronics and Semiconductor Technology, 419.
- [2] **Marciniak B., Różycka-Sokolowska E., Balińska A., Pawliuk W.**, Proc. SPIE, **4413**, International Conference on Solid State Crystals 2000: Epilayers and Heterostructures in Optoelectronics and Semiconductor Technology, 408.
- [3] **Marciniak B., Dziwiński E.**, Proc. SPIE, **4413**, International Conference on Solid State Crystals 2000: Epilayers and Heterostructures in Optoelectronics and Semiconductor Technology, 413.
- [4] **Marciniak B.**, Journal of Crystal Growth **241** (2002) 206.
- [5] **Kotula I., Marciniak B.**, Journal of Chem & Eng. Data, **46** (2001) 783.
- [6] **Probst K.-H., Karl N.**, Phys. Stat. Sol. A, **27** (1975) 499.
- [7] **Pope M., Swenberg C.E.**, Electronic Processes in Organic Crystals, Clarendon Press, Oxford, 1982.
- [8] **Bodzioch A., Marciniak B., Różycka-Sokolowska E., Jeszka J.K., Uznański P., Kania S., Kuliński J., Bałczewski P.**, Chem.-A Eur. J., **18** (2012) 4866.

PEWNE WŁASNOŚCI ELEKTRYCZNE CIENKICH WARSTW 9,10-DIMETYLOANTRACENU I 1-ACENAFTOLU

Streszczenie

Zbadano własności elektryczne materiałów o czystości spektralnej uzyskanych metodą dodatkowego oczyszczania strefowego komercyjnie dostępnych 1-acenaftolu i 9,10-dimetyloantracenu. Warstwy wymienionych związków, naporowywane w próżni 10^{-5} Tr, wykazywały wysoką oporność właściwą w granicach 10^{11} - 10^{12} $\Omega\cdot\text{m}$ i charakteryzowały się bardzo niską zawartością pułapek rzędu 10^{11} - 10^{14} cm^{-3} . Wyniki świadczą o stabilności molekuł badanych materiałów w warunkach naporowywania termicznego w próżni 10^{-5} Tr oraz o ich zdolności do łatwej nukleacji na złotych elektrodach. Warstwy wykazują stabilność rezystancji aż do wartości pola polaryzacji $2\cdot 10^7$ V/m.

**RAFAŁ LEDZION, MAREK IZDEBSKI, PIOTR GÓRSKI
WŁODZIMIERZ KUCHARCZYK**

Institute of Physics, Lodz University of Technology
ul. Wólczajska 219, 90-924 Łódź, Poland
e-mail: wlodzimierz.kucharczyk@p.lodz.pl

ESTIMATIONS OF THE MAGNITUDE OF THE FOURTH-ORDER ELECTROOPTIC EFFECT IN KDP-TYPE CRYSTALS

An attempt to measure the fourth-order electrooptic effect in KH_2PO_4 (KDP) and $NH_4H_2PO_4$ (ADP) is presented. Contrary to previously reported results of the order of magnitude $10^{-30} m^4V^{-4}$, the fourth-order coefficient $|g_{111111} - g_{221111}|$ is found to be lower than $5 \cdot 10^{-33} m^4V^{-4}$ and $1 \cdot 10^{-34} m^4V^{-4}$, respectively. In addition, the effect of imperfect crystal cutting and alignment is investigated by means of calculations based on Jones calculus. It is found that even small inaccuracies may lead to an apparent fourth-order electrooptic effect comparable in magnitude to the previously reported values.

Keywords: fourth-order electrooptic effect, KH_2PO_4 , $NH_4H_2PO_4$.

1. INTRODUCTION

Results of measurements of the fourth-order electrooptic coefficients have been previously reported for some crystals including $BaTiO_3$ [1] and members of the KDP (KH_2PO_4) family (see, e.g. [2-4]). The first published results for the fourth-order effect in KDP type crystals have been obtained employing static fields and indicate very large values of the order of magnitude $10^{-30} m^4V^{-4}$. However, these results have not been confirmed by further attempts to measure the effect by dynamic means [5,6]. One notes that somewhat similar situation may be observed for the quadratic electrooptic effect, where apparent coefficients obtained by static methods and due to an imperfectly cut or aligned crystal are sometimes three orders of magnitude larger than results of dynamic

measurements [7,8]. The theoretical results presented recently for the quadratic electrooptic effect have shown that the sensitivity of measurements performed by static means for the inaccuracies is much higher than in methods employing a sinusoidal electric modulating field. Corresponding nonlinearities may lead to apparent nonlinear electrooptic effects [9-11].

The fourth-order effect is important from the point of view of the relationship between the spontaneous birefringence and spontaneous antipolarization in the low-temperature phase of $\text{NH}_4\text{H}_2\text{PO}_4$ (ADP) [12]. One notes that a significant contribution of the fourth-order electrooptic effect would affect this relationship. Thus, nonlinear electrooptic properties of ferroelectric and antiferroelectric crystals are of interest as related to the nature of the spontaneous birefringence in their low-temperature phases. Moreover, the fourth-order electrooptic effect is important in analyses of the temperature dependencies of intrinsic (*i.e.* defined in terms of polarization) quadratic electrooptic coefficients in ferroelectrics and ferroelectrics [16]. Nonlinear electrooptic effects may also lead to nonlinear responses of various technical devices employing electrooptic crystals, therefore, are important in applications.

The aim of this work is to investigate the magnitude of the fourth-order electrooptic coefficient $g_{111111} - g_{221111}$ in KDP and ADP crystals.

2. EXPERIMENTAL

We have employed the dynamic polarimetric technique described previously (see, e.g. references [12,13]) and based on the harmonic analysis of light modulated by the sinusoidal modulating voltage $U(t) = U_0 \sin(\omega t)$ using the electric field of frequency 417 Hz. Such a frequency is much lower than any piezoresonance frequency in our samples, so that the crystals resting freely on their supports could be regarded as mechanically free. The samples under investigation were positioned so that the He-Ne laser beam propagated along their optical axes. Measurements were made for several such light paths across the entrance face of each crystal. The modulator used in measurements was biased to the middle of its transmission characteristic by a quarter-wave plate. To apply the electric field parallel to the [100] direction, the faces of samples were coated with conducting silver paint. The samples were placed in a bath containing a silicon oil having checked previously that the contribution of its Kerr effect due to the fringing field is negligible. The measurements were performed at temperature 295 K. The use of the lock-in amplifiers enabled sensitive measurements of the response of the system to be made on frequencies

ω , 2ω and 4ω . The readings on the fundamental frequency ω were useful to provide precise orientations of the investigated crystals. Our measurements were made on crystals with dimensions $50 \times 50 \times 5 \text{ mm}^3$.

For the configuration under consideration and in the absence of any errors in crystal cutting or alignment the electric field induced birefringence in crystals belonging to the point symmetry $\bar{4}2m$ group is given as [14]

$$\Delta n(t) \approx \frac{n_o^3}{2} \left[(g_{1111} - g_{2211}) E(t)^2 + (g_{111111} - g_{221111}) E(t)^4 \right], \quad (1)$$

where n_o is the ordinary refractive index and g_{ijkl} and g_{ijklmn} are components of the quadratic and fourth-order electrooptic tensors, respectively. Thus, the absolute value of the fourth-order coefficient $g_{111111} - g_{221111}$ is related to the response $U(4\omega)$ of the modulator used in measurements on the fourth harmonic by

$$|g_{111111} - g_{221111}| = \frac{8\lambda d^4 U(4\omega)}{\pi n_o^3 l U_c U_0^4}, \quad (2)$$

where d is the crystal thickness, l its length and U_c is the voltage measured the constant component of the light intensity.

With sensitivity of our apparatus allowing to detect the fourth-order electrooptic coefficient $|g_{111111} - g_{221111}|$ of magnitude $2 \cdot 10^{-34} \text{ m}^4 \text{V}^{-4}$ and $1 \cdot 10^{-34} \text{ m}^4 \text{V}^{-4}$, for KDP and ADP, respectively, we have not been able to observe any response. Thus, this effect should be lower.

3. THE APPARENT FOURTH-ORDER ELECTROOPTIC EFFECT

In real measurements some inaccuracies in crystal cutting and alignment may appear. To explain the discrepancy between our results and the former obtained by static means, we have performed computer simulations of measurement conditions of the fourth-order coefficients. In this we have followed the approach employed previously for the linear and quadratic electrooptic effects [8-11,15]. We have applied the Jones calculus for a modulated double-refracted light beam propagating in an electrooptic uniaxial crystal [11] employing the angles describing the inaccuracies as shown in Fig. 1. Examples of our results obtained for the fourth-order apparent electrooptic effect are plotted in Fig. 2.

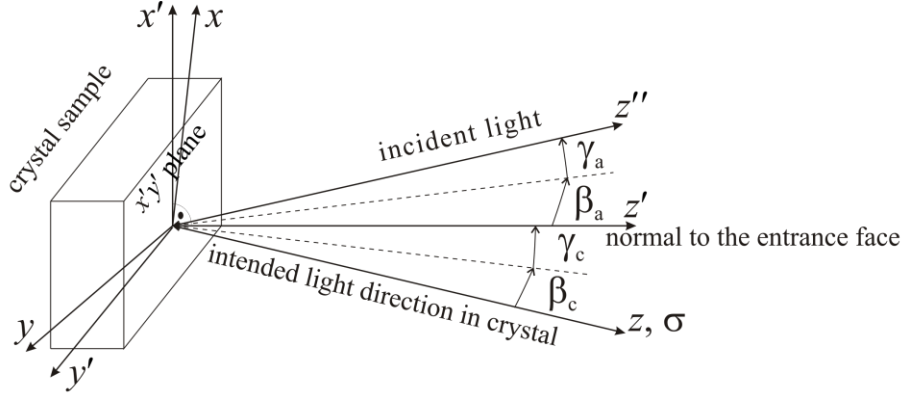


Fig. 1. Definition of the angles β_c and γ_c describing the inaccuracies in the crystal cutting and β_a and γ_a related to its inaccurate alignment

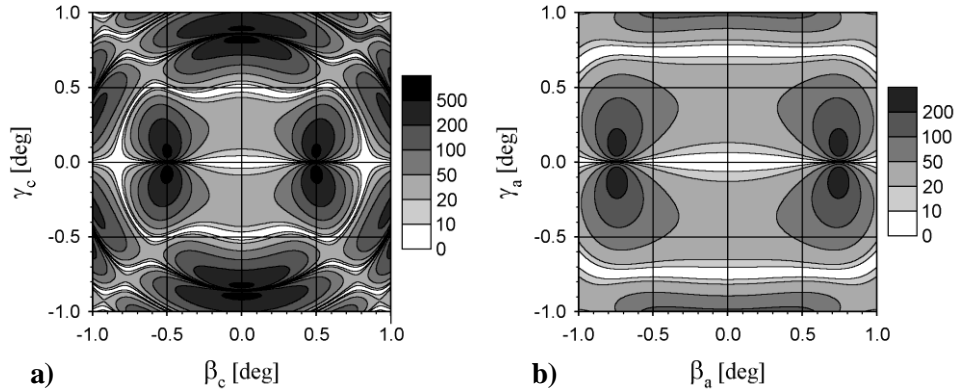


Fig. 2. Calculated values of the apparent fourth-order coefficient $|g_{111111} - g_{221111}|$ in $10^{-33} \text{ m}^4 \text{ V}^{-4}$ in KDP obtained by assuming the use of the static electric field of strength up to 10^6 Vm^{-1} . The radius of the light beam of the uniform intensity is 0.5 mm, the wavelength $\lambda = 0.63 \mu\text{m}$ and the crystal length is $l = 5 \text{ cm}$. The intended directions of the light beam and the electric field are $\sigma = (1,0,0)$ and $\mathbf{E} = (E,0,0)$. Considered examples: a) inaccuracies in the crystal cutting in the absence of inaccuracies in the crystal alignment, b) inaccuracies in the crystal alignment in the absence of inaccuracies in the crystal cutting

4. DISCUSSION

In our opinion, earlier results that are not confirmed by our measurements stem from the lower-orders electrooptic effects in the presence of inaccuracies in the alignment or cutting of investigated samples. The plots presented in Fig. 2 suggest that analogously to some earlier measurements of the quadratic electrooptic effect, the previously determined very large fourth-order coefficients are apparent not the real ones.

REFERENCES

- [1] Meyerhofer D., *Phys. Rev.*, **112** (1958) 413.
- [2] Perfilova V.E., Sonin A.S., *Izv. Akad. Nauk SSSR, Ser. fiz.*, **31** (1967) 1136.
- [3] Perfilova V.E., Sirotnin Yo., Sonin A.S., *Kristallografiya*, **14** (1967) 157.
- [4] Sonin A.S., Vasilevskaya A.S., *Electrooptic Crystals*, (in Russian) Atomizdat, Moscow (1971).
- [5] Jamroz W., Karniewicz J., *Opt. Quant. Electron.*, **11** (1979) 23.
- [6] Górski P., Kucharczyk W., *phys. stat. sol. (a)*, **121** (1990) K243.
- [7] Gunning M.J., Kucharczyk W., Raab R.E., *J. Opt. Soc. Amer. B*, **18** (2001) 1092.
- [8] Izdebski M., Kucharczyk W., Raab R.E., *J. Opt. Soc. Amer. A*, **19** (2002) 1417.
- [9] Izdebski M., Kucharczyk W., Raab R.E., *J. Opt. A: Pure Appl. Opt.*, **5** (2003) 147.
- [10] Izdebski M., Kucharczyk W., *Optica Applicata*, **33** (2003) 213.
- [11] Izdebski M., Kucharczyk W., Raab R.E., *J. Opt. Soc. Amer. A*, **21** (2004) 132.
- [12] Ledzion R., Bondarczuk K., Kucharczyk W., *Cryst. Res. Technol.*, **39** (2004) 161.
- [13] Ledzion R., Górski P., Bondarczuk K., Kucharczyk W., *Cryst. Res. Technol.*, **34** (1999) 745.
- [14] Jamroz W., Karniewicz J., Kucharczyk W., *J. Phys. D: Appl. Phys.*, **11** (1978) 2625.
- [15] Izdebski M., Kucharczyk W., Raab R.E., *J. Opt. Soc. Amer. A*, **18** (2001) 1393.
- [16] Ledzion R., Izdebski M., Bondarczuk K., Kucharczyk W., *Opto-Electron. Rev.*, **12** (2004) 449.

PRÓBA WYZNACZENIA WIELKOŚCI ELEKTROOPTYCZNEGO EFEKTU CZWARTEGO RZĘDU W KRYSZTAŁACH GRUPY KDP

Streszczenie

Wykorzystując dynamiczną metodę polaryzacyjno-optyczną przeprowadzono próbę pomiaru elektrooptycznego efektu czwartego rzędu w kryształach KH_2PO_4 (KDP) oraz $\text{NH}_4\text{H}_2\text{PO}_4$ (ADP). W przeciwieństwie do zmierzonych wcześniej przy wykorzystaniu metody statycznej i prezentowanych w literaturze wielkości współczynnika $|g_{111111} - g_{221111}|$ rzędu $10^{-30} \text{ m}^4\text{V}^{-4}$, otrzymane w pracy wyniki pozwalają stwierdzić, że współczynnik ten, odpowiednio dla kryształów KDP i ADP, jest mniejszy niż $5 \cdot 10^{-33} \text{ m}^4\text{V}^{-4}$ oraz $1 \cdot 10^{-34} \text{ m}^4\text{V}^{-4}$. Analizując przyczyny rozbieżności otrzymanych wyników i tych otrzymanych wcześniej, rozważono wpływ błędów w wycięciu i orientacji wykorzystanych próbek krystalicznych na wynik pomiarów. Wykorzystując rachunek Jonesa pokazano, że takie niedokładności mogą prowadzić do znaczących nieliniowości w odpowiedzi układu pomiarowego, sugerując istnienie pozornego efektu czwartego rzędu, który może być nawet o kilka rzędów wielkości większy niż efekt prawdziwy.

MAGDALENA WŁODARSKA, BARTOSZ SKURPEL

Institute of Physics, Lodz University of Technology
ul. Wólczajska 219, 90-924 Łódź, Poland
e-mail: magdaw@p.lodz.pl

CURING CONDITIONS AND DIELECTRIC OBSERVATION OF AN EPOXY SYSTEM BASED ON EPIDIAN 6

In this work the dielectric properties and curing conditions of a selected epoxy resin are presented. The curing system consists of Epidian 6 with DDM amine. In the first step, optimal curing conditions were determined for different amine concentrations in the mixture. It is shown on a diagram, how the properties of the cured matrix depend on the percentage concentration of the curing agent. Dielectric measurements were carried out for two concentrations – 10% and 16% – both in the course of curing and for the final product. Significant differences in the dielectric responses were observed as a result of different conversion levels in the obtained resins.

Keywords: epoxy network, curing conditions, dielectric properties.

1. INTRODUCTION

Epidian 6 belongs to epoxy resins – a group of materials which are widely used nowadays in many branches of the industry [1,2]. Studying the process of curing a selected material with certain curing agents and determining the curing conditions and properties of the final product are essential steps needed for successful application of that material. A series of papers [3-5] dedicated to the process of curing Epidian 6 with triethylenetetramine may serve as an example. Those papers presented diagrams describing changes in the physical properties of the mixture with respect to the curing conditions i.e. time and temperature. Our paper shows the results of curing Epidian 6 with the DDM amine. Depending on the amount of the used curing agent, different properties of the cured product were obtained. For amine concentration of 10% and 16% dielectric studies were carried out. Changes in the dielectric response clearly reflect different levels of chemical conversion in both the products.

2. MATERIALS

Mixtures prepared for the dielectric measurements were made of commercially available basic components: epoxy monomer Epidian 6 and DDM amine. The mixtures were prepared with different mass ratios of DDM amine: 8%, 10%, 12%, 14% and 16%. Observations of the mixture behaviour were conducted during slow heating up to the temperature of 160°C. For further analysis, mixtures with 10% and 16% amine concentrations were selected. The chosen samples were cured for 5 hours at the temperature of 70°C and post-cured at 160°C (for 10% amine concentration) or 120°C (for 16% concentration). In situ monitoring of the dielectric response was carried out during the process of curing.

3. EXPERIMENTAL

The optical observations of the mixtures were done using a microscope at a magnification of 80×. The material was deposited on plain glass plates.

Dielectric monitoring of curing was performed for samples with thickness of 50 μm, placed between metal discs. The dielectric response was recorded using Solartron 1260 Impedance Analyser with Chelsea Dielectric Interface 1295. The real and imaginary components of capacitance were evaluated in the frequency range from 10⁻² to 10⁵ Hz. The temperature of the samples was stabilized with the accuracy of 0.2 K using Unipan 620 temperature controller. Dielectric analysis of the final products was performed in a wide range of frequency (10⁶-10⁻¹ Hz) in the cooling route, using the Alpha high-resolution dielectric analyzer manufactured by Novocontrol. Temperature was controlled by a Quatro cryosystem (Novocontrol) and data was collected after reaching thermal stabilization (with accuracy of 0.1 K).

4. RESULTS AND DISCUSSION

In the first step, a series of mixtures of Epidian 6 with DDM amine in different concentrations were monitored during heating up to the temperature of 120°C. Changes in physical properties were observed in the mixtures with 8%, 10%, 12%, 14% and 16% contents of the amine. After annealing the samples at 120°C all the mixtures were further heated up to the temperature of 160°C and changes occurring in the already reacted samples were observed.

The conclusions from the observations are shown on the diagram (Fig. 1). At 8% concentration of the amine, a viscous plastic mass was obtained, which completely melted after being heated up.

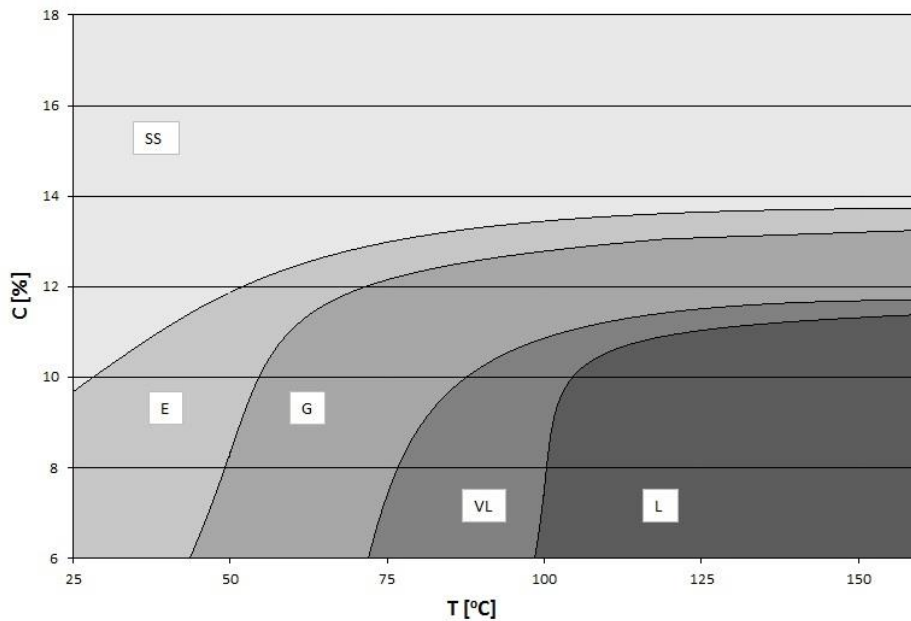


Fig. 1. Diagram showing varying degree of curing Epidian 6 with DDM amine, depending on the percentage concentration of the curing agent. Regions corresponding to different physical properties of the obtained product are indicated with different grey levels: SS – solid state, E – elastic, G – gel, VL – viscous liquid, L – liquid

For 10% and 12% mixtures, the curing product was solid at room temperature but became plastic after being heated up. Only for concentrations above 14% the obtained product was solid and non-plastic even at elevated temperatures.

For further dielectric measurements, the mixtures with 10% and 16% amine concentration were selected. The previously observed changes of the physical properties of the cured products at varying temperatures are also confirmed in the dielectric response (Figs. 2, 3 and 4). Differences in the progress of the curing process were clearly seen already during dielectric monitoring of that process (Fig. 2).

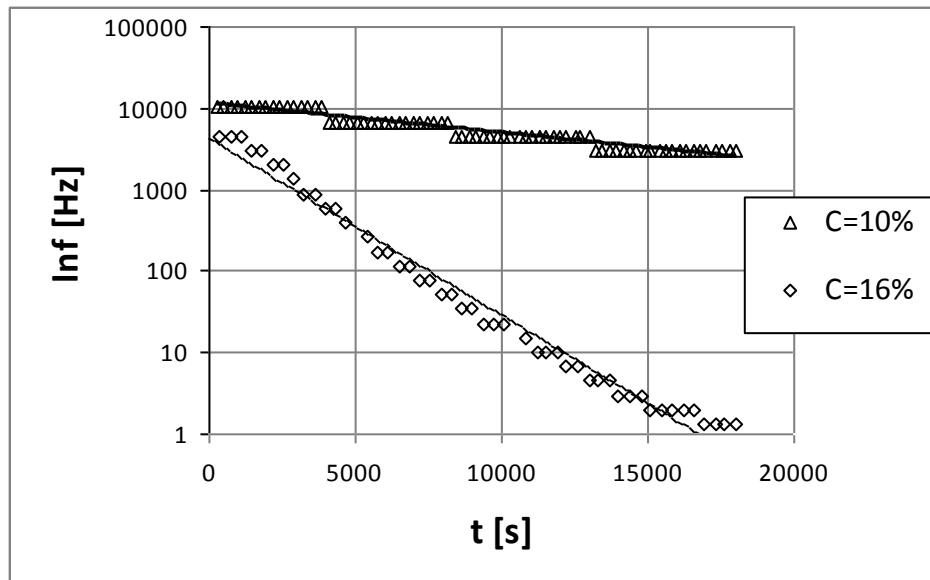


Fig. 2. Logarithmic plot of the electric modulus' imaginary component's peak frequency against time for two different mixtures with 10% and 16% concentration of the DDM amine

Fig. 2 presents changes in the peak frequency of the imaginary component of the electric modulus with time. That peak is directly related to the DC conductivity of given material. Therefore, changes observed in Fig. 2 reflect the nature and rate of conductivity changes in the dielectric material. The plot clearly shows that the reaction runs slower in the mixture with 10% amine concentration and the conductivity of that material does not reach the same value as in the other mixture – even though the initial values of the conductivity are similar and curing takes place at the same temperature of 70°C. As a result, both materials have quite different physical properties after being heated up which is a confirmation of the earlier observations. The material with 16% amine concentration did not reach a stable, constant final value before the end of the measurements. This leads to a conclusion that the curing time was too short for achieving full conversion of the mixture. Consequently, additional annealing at a higher temperature was done in the second phase of the investigations to let the reaction run to completion. The annealing was applied to both the mixtures and full stabilization was observed after some time in both the cases. In the next step, dielectric response was recorded for both the cured products in a wide range of frequency and temperature (Figs. 3 and 4).

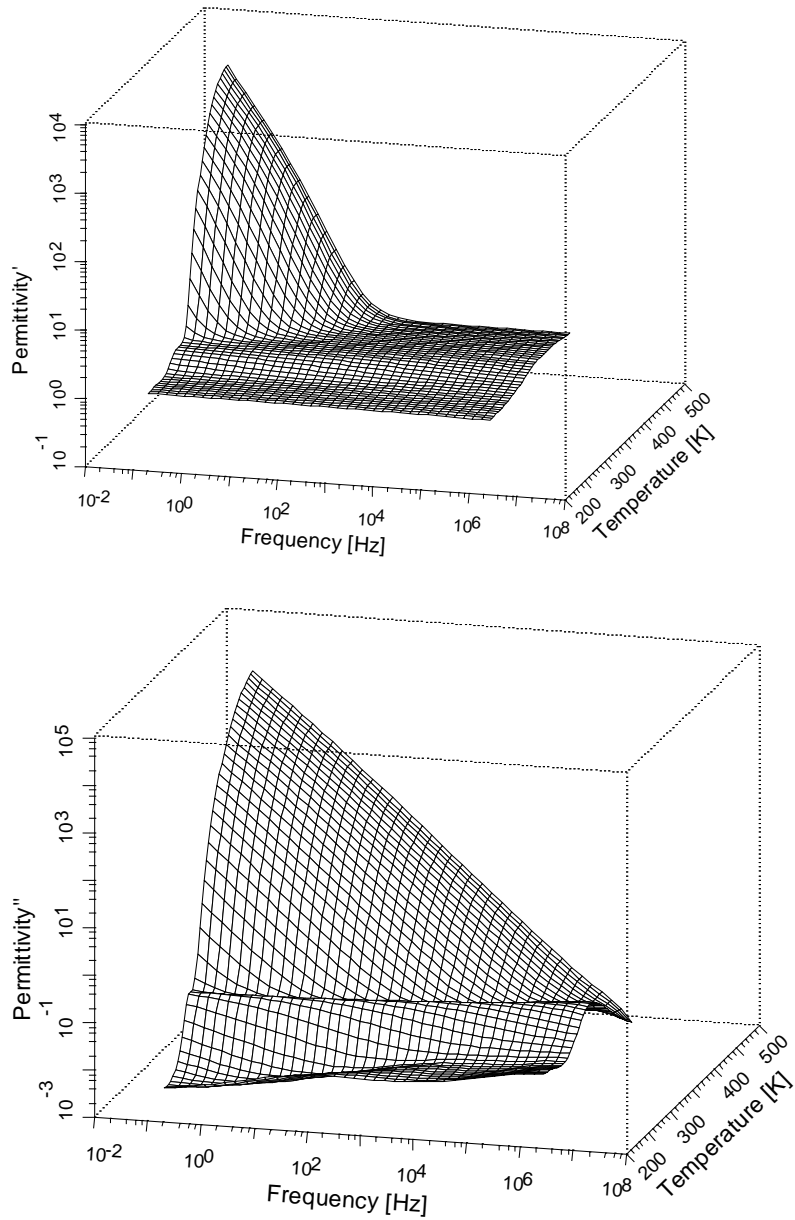


Fig. 3. Dependency of the real (a) and imaginary (b) component of the electric permittivity on frequency in a broad range of temperature, for a cured mixture with 10% concentration of DDM amine

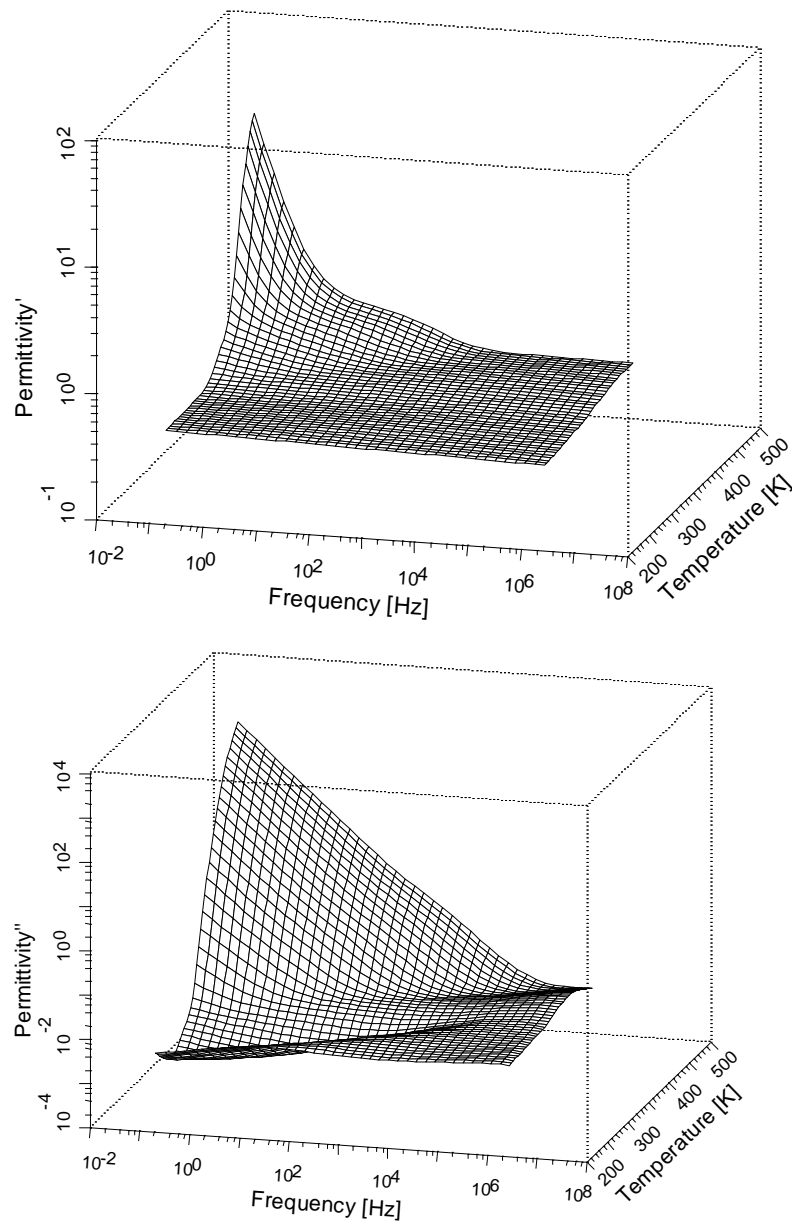


Fig. 4. Dependency of the real (a) and imaginary (b) component of the electric conductivity on frequency in a broad range of temperature, for a cured mixture with 16% concentration of DDM amine

Figs. 3 and 4 show 3D plots of the real and imaginary components of the electric permittivity, plotted against frequency and temperature. The same rapid growth of electric permittivity at low frequencies and elevated temperatures is present in both the figures. This growth is connected with similar electric conductivity of the two materials. Below the temperature of 400 K significant differences between the two materials can be noticed, particularly by comparing the plots of the imaginary component of the electric permittivity. In this case, an α -process related to molecular motions of whole polymeric structures clearly appears in the material with 10% amine concentration. This process becomes visible near the temperature of 353 K ($\sim 80^\circ\text{C}$) and its disappearance marks vitrification of the material which occurs at temperatures below 283 K ($\sim 10^\circ\text{C}$). No analogous process can be seen in the material with 16% amine concentration (Fig. 3) which means that a glass transition does not occur in that material in the studied range of temperatures. Another relaxation process can be observed at low temperatures (below 300 K) in both the materials. This process can be attributed to molecular motions of local polar groups.

5. CONCLUSIONS

The performed observations enabled determination of the optimal curing conditions and percentage composition of the mixture of Epidian 6 with the DDM amine. The dielectric measurements revealed differences both in the curing process and in the physical properties of two different cured products. In both cases, a relaxation process connected with mobility of local polar groups was detected. An additional process related to a phase transition was found in the material with lower concentration of the amine. It was noted that dielectric studies can be applied in order to determine appropriate curing conditions as well as to perform in situ monitoring of the curing reaction.

REFERENCES

- [1] Brojer Z., Hertz Z., Penczek S., *Żywice epoksydowe*, PWT, Warszawa 1960.
- [2] Czub P., Bończa-Tomaszewski Z., Pęczek P., Pieluchowski J., *Chemia i technologia żywic epoksydowych*, WNT, Warszawa 2002.
- [3] Urbaniak M., Grudziński K., *Polimery*, 52(4) (2007) 255.
- [4] Urbaniak M., *Polimery*, 53(7-8) (2008) 537.
- [5] Urbaniak M., Grudziński K., *Polimery*, 52(2) (2007) 117.

WARUNKI SIECIOWANIA I OBSERWACJE DIELEKTRYCZNE UKŁADU EPOKSYDOWEGO OPARTEGO NA EPIDIANIE 6

Streszczenie

W pracy przedstawiono właściwości dielektryczne oraz warunki sieciowania dla wybranej żywicy epoksydowej. Badany układ zawierał Epidian 6 oraz aminę DDM. W pierwszym kroku określono optymalne warunki sieciowania dla różnej procentowej zawartości aminy w mieszaninie. Na diagramie pokazano, jak właściwości usieciowanej matrycy zależą od procentowej zawartości utwardzacza. Pomiary dielektryczne wykonano dla dwóch mieszanin o zawartości 10% i 16% wagowych DDM podczas sieciowania, jak i po usieciowaniu. Zaobserwowano znaczące różnice w odpowiedzi dielektrycznej, co było wynikiem różnego stopnia utwardzenia badanej żywicy.

MAREK WOJCIECHOWSKI,^{1,2} MARZENA TYKARSKA³
GRZEGORZ W. BĄK²

¹Centre of Mathematics and Physics, Lodz University of Technology
Al. Politechnik i 11, 90-924 Łódź, Poland

²Institute of Physics, Lodz University of Technology
ul. Wólczajska 219, 90-924 Łódź, Poland

³Institute of Chemistry, Military University of Technology
ul. Kaliskiego 2, 00-908 Warsaw, Poland

DIELECTRIC PROPERTIES OF FERRIELECTRIC SUBPHASE OF LIQUID CRYSTAL MHPOPB

The antiferroelectric liquid crystal with relatively broad temperature range of ferrielectric subphase was chosen for dielectric investigations of this subphase. In the ferrielectric subphase, collective molecular motions were registered as a ferrielectric Goldstone mode. Theory of ferroelectric Goldstone mode was applied to the registered ferrielectric subphase to obtain rotational viscosity.

Keywords: dielectric relaxations, ferrielectric Goldstone mode.

1. INTRODUCTION

Antiferroelectric liquid crystals show not only antiferroelectric and ferroelectric phases, but frequently also the smectic chiral subphases. In the cooling process the following phases and subphases may appear: Iso \rightarrow SmA^{*} \rightarrow SmC^{*} \rightarrow SmC _{α} ^{*} \rightarrow SmC _{β} ^{*} \rightarrow SmC _{γ} ^{*} \rightarrow SmC_A^{*} \rightarrow Cr [1]. The subphases exist typically in a rather narrow temperature range as for standard antiferroelectric liquid crystalline material MHPOBC [2].

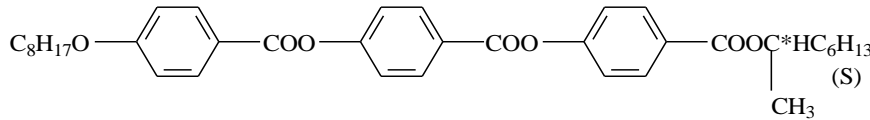
The temperature ranges of various subphases in MHPOPb proves to be substantially broader but it was not clear what phases and subphases does occur in this material. Kuczyński *et al.* [3] suggested that three various chiral smectic subphases occur in MHPOPb. Our earlier investigations [4] supported the suggestions by Kuczyński *et al.* The MHPOPb was investigated dielectrically in our earlier work [4].

The investigations were carried out in the cells with ITO electrodes. The results confirm existence of three subphases (SmC_α^* , SmC_β^* , SmC_γ^*) in this compound and especially broad range of ferrielectric SmC_γ^* phase.

In this work, the new dielectric investigations of MHPOPB were performed. For the presented investigations we used gold electrodes in order to avoid the influence of ITO electrodes on the dielectric response and to obtain more precise results. The present investigations are focused on dielectric characteristic of ferrielectric SmC_γ^* subphase. Theory of ferroelectric Goldstone mode has been applied for the observed ferrielectric subphase. The rotational viscosity has also been calculated from the results.

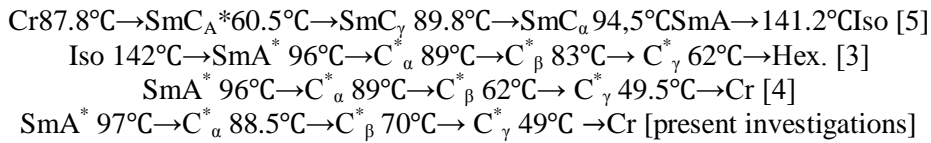
2. EXPERIMENTAL

Antiferroelectric liquid crystalline compound MHPOPB presented below, with relatively broad temperature range of ferrielectric subphase, has been investigated dielectrically:



The investigated compound was synthesized in the Institute of Chemistry, Military University of Technology (Warsaw) [5].

The phase sequence in the investigated compound has been reported to be as follows :



The dielectric measurements were performed for the liquid crystal compound placed between two parallel glass plates with 5×5 mm gold electrodes. We used standard cells, commercially available from AWAT. The used cells give planar orientation. The sample thickness was $d = 5 \mu\text{m}$. The measuring sinusoidal signal (0.1 V) was applied nearly perpendicularly to the director of smectic layers. The measurements were carried out with Solartron 1260 A Impedance Analyser with Chelsea Dielectric Interface in the frequency range $10^{-3} \text{ Hz} \div 5 \cdot 10^5 \text{ Hz}$.

The dielectric measurements were performed in cooling process of liquid crystal sample. The Havriliak-Negami equation was used for fitting the experimental results in the following version:

$$\varepsilon^*(\omega) = \varepsilon' - i\varepsilon'' = -i \left(\frac{\sigma_0}{\varepsilon_0 \omega} \right)^n + \sum_{k=1}^m \left\{ \frac{\Delta\varepsilon_k}{\left[1 + (i\omega\tau_k)^{\alpha_k} \right]^{\beta_k}} + \varepsilon_{\infty k} \right\}$$

where σ_0 – dc conductivity, $\Delta\varepsilon$ – dielectric strength, τ – relaxation time, α – width parameter, β – asymmetry parameter, ε_{∞} – infinite permittivity.

3. RESULTS AND DISCUSION

The temperature dependencies of the real part of dielectric permittivity at constant frequencies are shown in Fig. 1 for the MHPOPB compound. This temperature dependence reflects phase sequence upon cooling. Similar temperature dependence of the dielectric permittivity were obtained previously [4]. The phase transition from isotropic phase to chiral smectic subpphase SmC^*_α has been detected. The structure of this subphase is still discussed. The next subphase registered in the material is antiferroelectric SmC^*_β subphase [6].

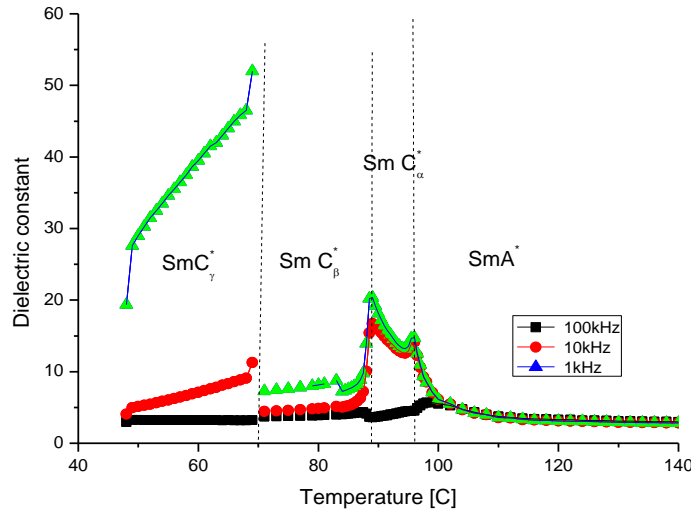


Fig. 1. Real part of dielectric permittivity vs. temperature for the whole temperature range investigated at chosen frequencies

In further cooling, the ferroelectric SmC_γ^* subphase appears. Only one relaxation mode was detected in each subphase.

The Havriliak-Negami equation was used for fitting the experimental data. Both the dielectric strength and the relaxation frequency of all registered relaxation processes are shown in Fig. 2.

In the SmC_α^* phase, some kind of phason is suggested to occur, its amplitude increases with increasing external dc field as it results from our earlier results [4]. The relaxation mode observed in the SmC_β^* phase, which has the antiferroelectric nature, was interpreted as azimuthal in anti-phase reorientation of the director with constant tilt. The ferroelectric Goldstone-like mode detected previously in the SmC_γ^* phase shows Arrhenius-like temperature dependence. The amplitude of this mode decreases with increasing dc bias like in the case of the typical ferroelectric Goldstone mode.

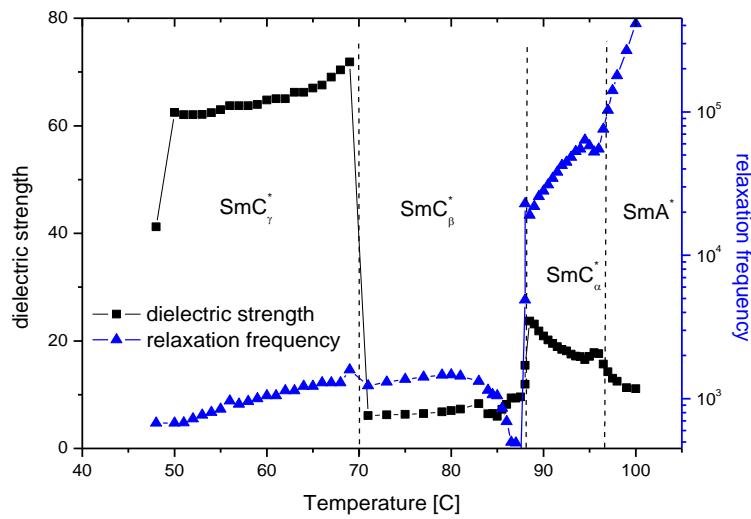


Fig. 2. Temperature dependence of dielectric strength and relaxation frequency of dielectric modes registered in MHPOPB

Theoretical description of Goldstone mode of ferroelectric phase is well known [7,8]. The theoretical formulae describing relaxation frequency and dielectric strength were used for classical ferroelectric Goldstone mode to determine Goldstone rotational viscosity [9-14].

In the ferroelectric phases, as predicted by generalized Landau model, the dielectric strength and the relaxation frequency of the Goldstone mode can be written as [7,8]:

$$\Delta\varepsilon_G = \frac{1}{2\varepsilon_0 K_{33} q^2} \left(\frac{P_S}{\theta} \right)^2$$

$$f_G = \frac{K_{33} q^2}{2\pi\gamma_G}$$

where K_{33} , γ_G , P_S , and θ are the elastic constant, the coefficient of rotational viscosity, the spontaneous polarization, and tilt angle respectively, $q = 2\pi/p$ is the helical wave vector of helical pitch p . From these equations the rotational viscosity γ_G constant could be calculated:

$$\gamma_G = \frac{1}{4\pi\varepsilon_0 \Delta\varepsilon_G f_G} \left(\frac{P_S}{\theta} \right)^2$$

The above formula was used to calculate the rotational viscosity related to ferrielectric-like Goldstone mode. The values of P_S and θ were taken from the work [3]. In the SmC_γ^* subphase, the unit cell consists of three layers but the polarisation of two of them is compensated and only every third layer gives rise to macroscopic polarisation. For this reason, the value of spontaneous polarisation obtained for SmC_γ^* subphase is divided by 3. In paper [15], the experimental results of the spontaneous polarisation in SmC_γ^* are presented. It is suggested that the values of the spontaneous polarisation in ferro- and ferri-subphases should be related as 3:1. The calculations were performed in the temperature range 60°÷70°C. In these temperatures the data necessary to calculate the Goldstone rotational viscosity are available in work [3]. In this temperature the calculated rotational viscosity changes from 113mPas at 60°C to 59mPas at 70°C in the SmC_γ^* phase of MHPOPB. It is risky to compare the calculated values of γ_G with other results for ferroelectric phases, because the value γ_G depends both on spontaneous polarization and dielectric strength, it depends also on temperature. There are a few values of γ_G available: 5÷10 mPas, Kuczyński *et al.* [9], 50÷300mPas, Goswami *et al.* [11], 70÷240 mPas, Hemine *et al.* [12].

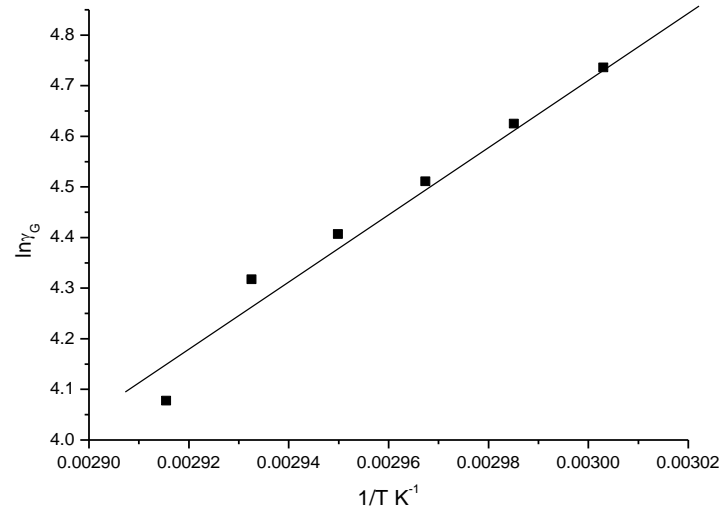


Fig. 3. Arrhenius plot of ferrielectric Goldstone rotational viscosity for MHPOPb. Values of ferrielectric Goldstone mode viscosity are taken in mPas

The Arrhenius law was used to evaluate of the rotational viscosity activation energy in the following formula:

$$\gamma_G = \gamma_0 \exp\left(\frac{E_A}{k \cdot T}\right)$$

where E_A is the activation energy. Plot of $\ln\gamma_G$ versus inverse of temperature is presented in Fig. 3 and shows linear behaviour. The obtained activation energy is equal 0.60 eV for ferrielectric SmC_γ^* subphase of MHPOPb.

The obtained activation energy differs a little from values obtained for ferroelectric phase of other materials: 0.32eV and 0.42eV for two compounds [14], and 0.51 for DOBAMBC [16]. However, the temperature dependence of γ_G in all the papers and in this work remains of Arrhenius type.

Though the calculated values of γ_G for the ferrielectric phase are close the values of γ_G found for ferroelectric phase of other materials, the applicability of generalized Landau model for ferroelectric phase of ferrielectric liquid crystalline materials is an open question.

CONCLUSIONS

1. The investigated MHPOPB antiferroelectric liquid crystal compound shows ferrielectric SmC_γ^* subphase in relatively broad temperature range.
2. The dielectric characteristic (*i.e.* the temperature dependence of both dielectric strength and relaxation frequency) in cells with gold electrodes are similar but not identical to those obtained in cells with ITO electrodes.
3. The ferroelectric theory of Goldstone mode was used to determine the ferrielectric Goldstone rotational viscosity. The obtained values of rotational viscosity should be treated as the first approximation, because it is difficult to estimate applicability of the model for ferroelectric subphase.
4. The obtained values of viscosity shows Arrhenius-type temperature dependence with activation energy equal to 0.60eV.

REFERENCES

- [1] Lagerwall J.P.F., Rudquist P., Lagerwall S.T., Giebelmann F., *Liq. Cryst.*, **30** (2003) 399.
- [2] Hou J., Schacht J., Giebelmann F., Zugenmaier P., *Liq. Cryst.*, **22** (1997) 409.
- [3] Kuczyński W., Goc F., Dardas D., Dąbrowski R., Hoffmann J., Stryła B., Malecki J., *Ferroelectrics*, **274** (2002) 83.
- [4] Wojciechowski M., Gromiec L.A., Bąk G.W., *J. Mol. Liq.*, **124** (2006) 7.
- [5] Dąbrowski R., Drzewiński D., Czupryński K., Gauza S., Kenig K., Kuczyński W., Goc F., *Mol. Cryst. and Liq. Cryst.*, **365** (2001) 199.
- [6] Górecka E., Pocięcha D., Cepic M., Zeks B., Dąbrowski R., *Phys. Rev. E*, **65** (2002) 061703.
- [7] Carlson T., Zeks B., Levstik A., Filipic C., Levstik I., Blinc R., *Phys. Rev. A*, **42** (1990) 87.
- [8] Singh A., Singh S., *Liq. Cryst.* **35** (2008) 727.
- [9] Kuczyński W., Dardas D., Nowicka K., *Phase Transitions* **82** (2009) 444.
- [10] Kuczyński W., Dardas D., Hoffmann J., Nowicka K., Jeżewski W., *Phase Transitions*, **85** (2012) 358.

- [11] Goswami D., Sinha D., Debnath A., Mandal P.K., Gupta S.K., Haase W., Ziobro D., Dąbrowski R., *J. Mol. Liquids*, **182** (2013) 95.
- [12] Hemine J., Daoudi A., Legrand C., El Kaaouachi A., Zazoui M., Isaert N., Nguyen H.T., *Spectroscopy Letters*, **41** (2008) 285.
- [13] Bousousalem Y., Ismaili M., Buisine J.M., Binet C., Joly G., Nguyen H.T., *Liq. Cryst.*, **36** (2009) 899.
- [14] Hemine J., Daoudi A., Legrand C., El Kaaouachi A., Nafidi A., Isaert N., Nguyen H.T., *M.J. Cond. Matter*, **12** (2010) 225.
- [15] Shytkov N.M., Vij J.K., Barnik M.I., Nguyen H.T., *Cryst. Reports*, **45** (2000) 682.
- [16] Levstik A., Kuntjak Z., Filipic C., Levstik I., Bregar Z., Zeks B., Carlsson T., *Phys. Rev. A* **42** (1990) 2204.

WŁASNOŚCI DIELEKTRYCZNE FAZY FERRIELEKTRYCZNEJ ZWIĄZKU CIEKŁOKRYSTALICZNEGO MHPOPБ

Streszczenie

Antyferroelektryczny związek ciekłokrystaliczny MHPOPБ posiadający szeroki temperaturowy zakres występowania fazy ferrielektrycznej, poddano badaniom dielektrycznym w komórkach o złotych elektrodach. Otrzymane dielektryczne charakterystyki związku są zbliżone do tych, które otrzymano we wcześniejszej pracy w komórkach z elektrodami ITO. Temperaturowe zależności częstości relaksacji i inkrementu dielektrycznego fazy ferrielektrycznej użyto do obliczenia rotacyjnej lepkości charakteryzującej ferrielektryczny mod Goldstone'a, analogicznie jak dla fazy ferroelektrycznej. Otrzymane wyniki dla fazy ferrielektrycznej są zbliżone do otrzymanych dla fazy ferroelektrycznej innych związków.

ISSN 1505-1013